



# Computational molecular spectroscopy

Vincenzo Barone<sup>1</sup>, Silvia Alessandrini<sup>1</sup>, Małgorzata Biczysko<sup>1</sup>, James R. Cheeseman<sup>1</sup>, David C. Clary<sup>4</sup>, Anne B. McCoy<sup>5</sup>, Ryan J. DiRisio<sup>5</sup>, Frank Neese<sup>6</sup>, Mattia Melosso<sup>1</sup> and Cristina Puzzarini<sup>1</sup>✉

**Abstract** | Spectroscopic techniques can probe molecular systems non-invasively and investigate their structure, properties and dynamics in different environments and physico-chemical conditions. Different spectroscopic techniques (spanning different ranges of the electromagnetic field) and their combination can lead to a more comprehensive picture of investigated systems. However, the growing sophistication of these experimental techniques makes it increasingly complex to interpret spectroscopic results without the help of computational chemistry. Computational molecular spectroscopy, born as a branch of quantum chemistry to provide predictions of spectroscopic properties and features, emerged as an independent and highly specialized field but has progressively evolved to become a general tool also employed by experimentally oriented researchers. In this Primer, we focus on the computational characterization of medium-sized molecular systems by means of different spectroscopic techniques. We first provide essential information about the characteristics, accuracy and limitations of the available computational approaches, and select examples to illustrate common trends and outcomes of general validity that can be used for modelling spectroscopic phenomena. We emphasize the need for estimating error bars and limitations, coupling accuracy with interpretability, touch upon data deposition and reproducibility issues, and discuss the results in terms of widely recognized chemical concepts.

<sup>1</sup>Scuola Normale Superiore, Pisa, Italy.

<sup>2</sup>International Centre for Quantum and Molecular Structures, Physics Department, Shanghai University, Shanghai, China.

<sup>3</sup>Gaussian Inc., Wallingford, CT, USA.

<sup>4</sup>Physical and Theoretical Chemical Laboratory, University of Oxford, Oxford, UK.

<sup>5</sup>Department of Chemistry, University of Washington, Seattle, WA, USA.

<sup>6</sup>Max-Planck-Institut für Kohlenforschung, Mülheim an der Ruhr, Germany.

<sup>7</sup>Department of Chemistry ‘Giacomo Ciamician’, University of Bologna, Bologna, Italy.

✉e-mail: [cristina.puzzarini@unibo.it](mailto:cristina.puzzarini@unibo.it)

<https://doi.org/10.1038/s43586-021-00034-1>

Spectroscopy is an experimentally non-invasive way of studying the electronic structure of a system in different environments and/or physico-chemical conditions to elucidate the system’s molecular structure, chemical linkages and reactivity. In this Primer, we consider medium-sized systems that include molecules ranging in dimension from a dozen atoms, such as the smallest amino acid glycine, to several tens of atoms, such as chlorophyll. We consider almost all possible environments, from gas phase to solution to crystals.

Among the various spectroscopic techniques<sup>1–5</sup>, rotational spectroscopy provides the most accurate and reliable information on the structure and dynamics of gas-phase molecules<sup>6–12</sup>. Although rotational spectroscopy is limited to the gas phase, vibrational spectroscopic techniques can investigate condensed phases to characterize molecules in terms of conformation, chemical linkage and mutual interactions among atoms and atomic charges modulated by temperature and environmental effects. For these reasons, vibrational spectroscopies such as infrared and Raman (as well as their chiral counterparts) are commonly employed to characterize the structure and dynamic behaviour of molecular systems. Finally, electronic spectroscopic techniques, in gas or condensed phases, deal with transitions between

different electronic states and characterize the molecular system in excited electronic states.

Modern high-resolution experimental spectroscopy may involve the acquisition of spectra resolving hundreds, if not thousands, of peaks, which is the case, for example, of rotational and ro-vibrational spectra of polyatomic, asymmetrical molecules as well as electron spin resonance (ESR) spectra of organometallic complexes. This spectral overcrowding means that the interpretation of high-resolution spectra without the help of quantum chemistry is a daunting, if not impossible, task. Indeed, computational spectroscopy, born as a branch of quantum chemistry for providing predictions of spectroscopic properties and features, evolved as an independent field. Currently, theoretical studies in the field of molecular spectroscopy play three roles: interpretation, complementarity, and prediction and support of experimental results. Computational spectroscopy exploits theoretical models, provides tools and computer codes, and validates procedures for the prediction, analysis, interpretation and understanding of spectroscopic features, properties and/or phenomena. Several aspects contribute to make computational spectroscopy an unavoidable tool in the field of molecular spectroscopy. As there is no room for addressing them all in detail<sup>13–18</sup>,

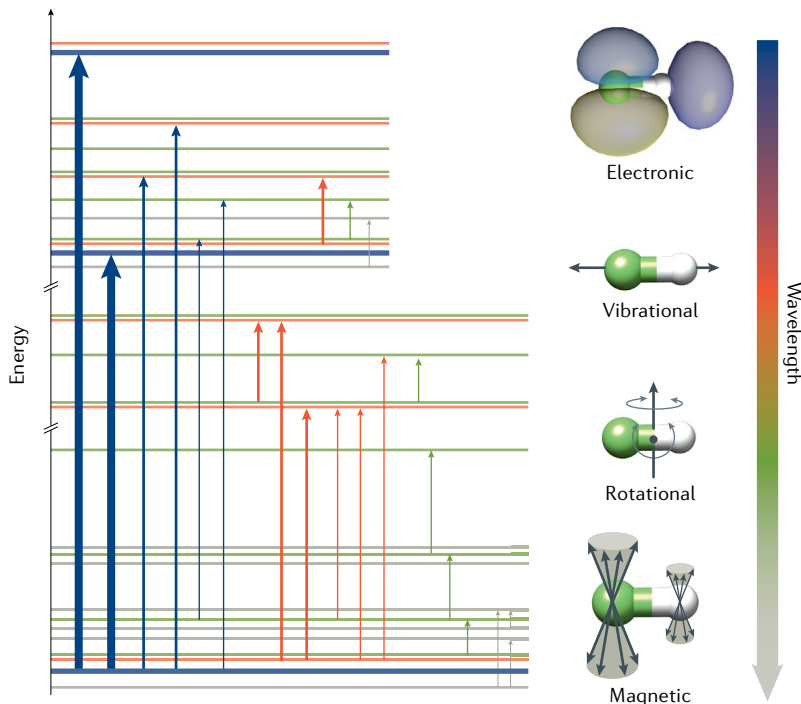


**Fig. 1 | Schematic representation of molecular energy levels and types of possible transitions.** Energy levels are obtained from the resolution of the Schrödinger equations. Blue arrows denote the transitions involving a change in the electronic state (from left to right, thicker to thinner: electronic, vibronic and rovibronic transitions). Red arrows denote the transitions involving different vibrational states (from left to right: vibrational and ro-vibrational transitions). Green arrows denote the transitions only involving rotational energy levels. Dark grey arrows denote the transitions between energy levels obtained from magnetic field splitting.

**Rotational spectroscopy**  
Spectroscopy using the microwave region of the electromagnetic field to study the excitation of the rotational states of molecules.

**Electron spin resonance**  
A spectroscopic technique equivalent to NMR but dealing with excitation of the electronic spins in open-shell systems.

**Quantum chemistry**  
The application of quantum mechanics to chemistry.

**Conformers**  
Isomers that can be converted into another by rotation about a formally single bond.

**Mössbauer isomer shifts**  
Shifts in resonance frequency of the nuclear gamma-ray transition in a Mössbauer active isotope (for example,  $^{57}\text{Fe}$ ) caused by its interaction with the molecular environment.

in the following we emphasize the topics we consider of primary importance.

In terms of spectral interpretation, spectroscopic experiments often need a broad computational investigation. For example, in order to analyse a recorded rotational or vibrational spectrum of flexible molecular systems, a computational conformational analysis as well as subsequent spectral predictions and simulations are necessary to understand which conformers contribute and how. Quantum chemistry also helps identify which aspects of a given structure are responsible for a specific spectroscopic property. Computational studies can establish structure/property relationships as they allow the on or off switching of specific effects and the analysis of the impact of these changes on the simulated spectrum. To give an example, in organometallic complexes, there is a strong relationship between metal–ligand bond distances and Mössbauer isomer shifts. Combining broad computational studies with a focus on structure–property relationships can, for example, identify short-lived and unstable species (in either ground or excited states).

In terms of complementarity, one of the goals of experimental spectroscopy is to understand the structure and bonding in molecules, although what is actually measured are the frequencies of light that are absorbed by the molecular system. Computational spectroscopy can act as a bridge between experiments and underlying physical properties, as it provides the theoretical expressions linking observable measurements and molecular

properties. Computational and experimental spectroscopy can also be used to benchmark each other<sup>19</sup>. As experimental spectroscopy is extremely sensitive to the electronic structure of a given system, it is one of the best ways to verify the reliability and accuracy of theoretical predictions and validate quantum chemistry calculations. In parallel, experimentally accessible spectroscopic properties may be much more sensitive to molecular structure than total energies, which are often not experimentally measurable.

In terms of prediction and support, the combination of theory and experiment provides experimentally calibrated or experimentally guided insights into electronic structure and can serve as a guide to the reactivity of systems. The prediction and interpretation of the structural properties and dynamic behaviour of molecules is at the heart of a deeper understanding of their stability and chemical reactivity. Furthermore, understanding electronic structure and how it is reflected in spectroscopic properties can give insights into entire classes of compounds, rather than only individual molecules. Computational spectroscopy can also act as the link between different experimental techniques that have traditionally been analysed separately, such as, for example, infrared spectroscopy, Raman spectroscopy, resonance Raman spectroscopy, UV–Vis absorption or fluorescence spectroscopy (as well as their chiral counterparts) and ESR. Quantum chemistry computations yield direct information on many properties of molecular systems to link molecular properties measured using different experimental techniques. Finally, although peak positions and intensities provide information on the structure of the system, the spectral line shape is related to dynamic aspects, such as fluctuations. As a consequence, vis-à-vis comparison between simulated and experimental spectra also gives access to these features.

FIGURE 1 provides a schematic representation of the types of transitions between molecular energy levels involved in the rotational, vibrational and electronic spectroscopies addressed in this Primer. In FIG. 1, and more generally in this Primer, the approach we follow to obtain the energy levels is based on effective Hamiltonians and the resolution of the corresponding Schrödinger equation. In addition to the spectroscopic techniques mentioned above and their chiral counterparts, we also consider magnetic resonance spectroscopies and a different computational approach for rotational and vibrational spectroscopies denoted diffusion Monte Carlo (DMC). FIGURE 1 also shows the physical aspects underlying each spectroscopic technique. For instance, rotational spectroscopy is related to the rotational motion of the molecular system under consideration, and can thus only be carried out experimentally in the gas phase. By contrast, vibrational spectroscopy describes the vibrational motion of the atoms within the molecule, and can therefore also be exploited in condensed phases.

In this Primer, we first provide, in Experimentation, the theoretical foundations and computational requirements of the spectroscopic techniques mentioned above. In Results, we present some specific results for these spectroscopic techniques, such as the derivation of structural information and the determination

**Infrared spectroscopy**

Spectroscopy using the infrared region of the electromagnetic field to study the excitation of the vibrational states of molecules.

**Raman spectroscopy**

Rotational or vibrational spectroscopy that exploits the Raman effect (inelastic scattering).

**Schrödinger equation**

Equation associated with the Hamiltonian operator: its resolution provides the allowed energy levels (eigenvalues) and the corresponding wave functions (eigenfunctions).

**Diffusion Monte Carlo**

A Monte Carlo-based approach for obtaining the exact ground-state solution to Eq. 2.

**Absolute configuration**

The spatial arrangement of atoms in a chiral system and its stereochemical description.

**Energy levels**

According to quantum mechanics (see above), the allowed energy for a system bound is not continuous but discretized in energy levels.

**Hamiltonian**

In quantum mechanics, the operator corresponding to the energy of a system.

**Position arrays**

Arrays containing the coordinates of the position of a specific point in a multidimensional space.

**Wave function**

A mathematical description of the quantum state of an isolated quantum system resulting from solving the corresponding Schrödinger equation.

**Born–Oppenheimer approximation**

The assumption that the motion of atomic nuclei and electrons can be treated separately, based on the much larger mass of nuclei.

**Potential energy surface**

A multi-dimensional, hyper-surface that describes the variations of the electronic energy of a system in terms of suitable nuclear coordinates.

of the absolute configuration of chiral molecules. In Applications, we select significant and varied examples of computational spectroscopy ranging from astrochemical studies to the characterization of biomolecules and transition metal complexes. We also address issues of Reproducibility and data deposition and some Limitations and optimizations of computational techniques before looking at some of the likely future directions in the field of computational spectroscopy.

**Experimentation**

In the framework of a Primer dedicated to computational spectroscopy, we translate the instrumentation, experimental design and equipment to the language of the computational world and discuss theoretical foundations, computational requirements and codes. In this section, we start with the theory underlying the spectroscopic phenomena associated with molecular systems, attempting to keep the treatment of mathematical expressions as simple as possible. We then move to the computational requirements needed to reach the desired accuracy. We conclude the section with a schematic presentation of some representative computer codes that are currently employed in the field of computational spectroscopy.

**Theoretical foundations**

The goal of computational spectroscopy is to couple accurate theoretical results with the interpretation of the experimental outcomes using well-defined models. Theoretical analysis of spectroscopic phenomena is related to the transitions between the energy levels ( $E_{\text{mol}}$ ) of a given molecule (FIG. 1), which can be obtained from the solution of the corresponding time-independent Schrödinger equation:

$$\hat{H}_{\text{mol}}(\mathbf{r}, \mathbf{R})|\Psi(\mathbf{r}, \mathbf{R})\rangle = E_{\text{mol}}|\Psi(\mathbf{r}, \mathbf{R})\rangle \quad (1)$$

where  $\hat{H}_{\text{mol}}(\mathbf{r}, \mathbf{R})$  is the molecular Hamiltonian (that is, the Hamiltonian associated with the molecular system under consideration), with  $\mathbf{R}$  and  $\mathbf{r}$  being the position arrays of the nuclei and electrons, respectively;  $|\Psi(\mathbf{r}, \mathbf{R})\rangle$  is the wave function denoting the state of the molecule. As Eq. 1 is unsolvable for the majority of the molecular systems, approximations must be introduced in order to obtain energy levels. The Born–Oppenheimer approximation<sup>20</sup> permits the separation of nuclear and electronic motions, thus leading to electronic and nuclear Schrödinger equations. Once nuclear and electronic motions are separated, a further approximation is required to simplify the nuclear Schrödinger equation. This is provided by the Eckart–Sayvetz conditions<sup>21,22</sup>, which factor out the translational motion and minimize the couplings between vibrations and rotations. One of the major consequences of the Born–Oppenheimer approximation is the concept of a potential energy surface (PES), which is a function of the nuclear coordinates and provides the relationship between the electronic energy of a molecule (from the resolution of the electronic Schrödinger equation) and its geometry. Stable molecular structures, also referred to as equilibrium structures, are minima on the PES. A mathematical description of the PES enters the Hamiltonian of the nuclear Schrödinger equation and, to simplify the

treatment, it is often expressed in terms of force constants, which are the derivatives of the electronic energies with respect to nuclear coordinates evaluated at the minimum.

Here, we focus on the nuclear Schrödinger equation and present its resolution by means of perturbation theory techniques. The advantage of perturbation theory is that it is generally accurate, and is a powerful interpretative tool allowing a direct connection with the parameters that are used by experimentalists to fit their spectra. The most common approach for considering nuclear quantum effects and obtaining the energies and wave functions needed to study spectroscopic properties involves solving the time-independent Schrödinger equation:

$$\hat{H}_{\text{vr}}(\mathbf{R})|\Psi_{\text{vr}}(\mathbf{R})\rangle = E_{\text{vr}}|\Psi_{\text{vr}}(\mathbf{R})\rangle \quad (2)$$

with the Watson Hamiltonian<sup>23</sup>  $\hat{H}_{\text{vr}}$  being the most widely used Hamiltonian for the description of the vibro-rotational motion of semi-rigid molecular systems. The Watson Hamiltonian is expressed in terms of the dimensionless normal coordinates  $q$  and their conjugate momenta  $\hat{p}$ . To minimize the rotational–vibrational coupling, the reference frame (principal inertia system) is centred in the centre of mass and oriented to diagonalize the equilibrium inertia tensor to fulfil the Eckart–Seyvetz conditions:

$$\begin{aligned} \hat{H}_{\text{vr}} = & \frac{1}{2} \sum_{\alpha, \beta} (\hat{J}_\alpha - \hat{\pi}_\alpha) \mu_{\alpha\beta} (\hat{J}_\beta - \hat{\pi}_\beta) + \frac{1}{2} \sum_r \omega_r \hat{p}_r^2 \\ & + V(q) - \frac{1}{2} \sum_\alpha \mu_{\alpha\alpha} \end{aligned} \quad (3)$$

The normal coordinates  $q$  are linear combinations of the displacements of the Cartesian coordinates of the atoms.  $\omega_r$  is the harmonic wavenumber associated with the  $r$ th normal coordinate, and  $\mu_{\alpha\beta}$  denotes an element of the inverse inertia tensor.  $\hat{J}_\alpha$  is the rotational angular-momentum operator about axis  $\alpha$ , and  $\hat{\pi}_\alpha$  represents the  $\alpha$ th component of vibrational angular momentum. As the exact form of the inverse molecular inertia tensor  $\mu$  and the potential energy  $V$  are unknown, they are expanded as Taylor series with respect to  $q$  about the equilibrium geometry. A detailed account can be found in REFS<sup>23,24</sup>.

A different procedure is offered by a Hamiltonian-independent approach based on inverting the information contained in the experimental spectroscopic transitions in order to derive the corresponding energy levels. After collecting all available (experimentally) measured transitions and selecting the most accurate data, such as those affected by the smallest errors, and compiling them into a database, spectroscopic networks are established in order to interconnect the energy levels. A spectroscopic network is a graph where the nodes are the energy levels and the links are the transitions. Inversion of the transitions through a weighted least squares-type procedure results in the energy levels and associated uncertainties. The MARVEL (measured active rotational–vibrational energy levels) protocol in the field of ro-vibrational spectroscopy<sup>25,26</sup> provides an illustrative example.

**Rotational spectroscopy.** The first step to addressing rotational spectroscopy is the definition of a suitable Hamiltonian. The starting point is the Watson

**Normal coordinates**

Linear combinations of mass-weighted displacement coordinates (usually Cartesian). The motion described by a normal coordinate is called a normal mode.

**Spectroscopic transitions**

The passage between two energy levels, that is, from an initial to a final state, detected by a spectroscopic technique.

**Ro-vibrational spectroscopy**

Spectroscopy dealing with rotational and vibrational states of molecules.

**Contact transformation**

Unitary transformation with an exponential operator  $U = \exp(iS)$ , where  $S$  is Hermitean and antisymmetrical with respect to time reversal, thus ensuring that  $U$  is unitary and invariant to time reversal.

**Anharmonic**

Deviation from the harmonic-oscillator behaviour.

**Hyperfine structure**

Interactions of the molecular electric and/or magnetic fields with the nuclear or electron (for open-shell species) moments produce a splitting of the rotational energy levels, which in turn leads to a splitting of the rotational transitions. This splitting is called the hyperfine structure.

**Coriolis couplings**

Interactions between the angular momentum of a vibrational mode and the rotational angular momentum.

**Rigid-rotor harmonic-oscillator model**

A reference model in which a molecular system as a whole is described in terms of a rigid rotating object and in terms of decoupled harmonic oscillators for its vibrational motion.

**Fundamental bands**

Vibrational transitions from the vibrational ground state to the first excited state of a given vibrational mode (a one-quanta transition).

**Vibrational circular dichroism**

Vibrational version of circular dichroism.

**Vibrational perturbation theory to the second order**

Exploitation of perturbation theory to the second order to treat vibrational motions.

Hamiltonian, from which we extract the rotational part. To accomplish this, we apply a contact transformation to the vibro-rotational Hamiltonian in Eq. 2 to obtain a block-diagonal effective Hamiltonian<sup>27</sup>. Each of these blocks is labelled in terms of the powers of  $q$  and  $\hat{p}$ , and of  $\hat{J}$ : the power of  $q$  and  $\hat{p}$  (vibrational) is referred to as  $n$  and that of  $\hat{J}$  (rotational) as  $l$ . Thus, the vibro-rotational Hamiltonian is now indicated as  $\hat{H}_{nl}$ . By retaining the pure rotational and centrifugal distortion terms where all Hamiltonian terms have  $n=0$ , we obtain the rotational Hamiltonian:

$$\tilde{H}_{\text{rot}} = H_{02} + \tilde{H}_{04} + \tilde{H}_{06} \quad (4)$$

where  $\tilde{H}_{04}$  and  $\tilde{H}_{06}$  are the quartic and sextic centrifugal distortion terms, and  $H_{02}$  is the rigid-rotor Hamiltonian:

$$H_{02} = \sum_i B_i^{\text{eq}} \hat{j}_i^2 \quad (5)$$

where  $\hat{j}_i$  is the projection of the rotational angular momentum operator along the  $i$ th inertial axis, and the  $B_i^{\text{eq}}$  terms represent the equilibrium rotational constants. The  $B_i^{\text{eq}}$  terms are inversely proportional to the corresponding components of the inertia tensor, which is diagonal in the principal inertia system, and only depends on the equilibrium structure and the isotopic masses of the atoms forming the molecule under consideration<sup>28</sup>. From a computational point of view, equilibrium rotational constants are derived from geometry optimization, the computational procedure that leads to the identification of the equilibrium structure. The accuracy of the equilibrium rotational constants therefore depends on the accuracy of this procedure.

To provide a description of the rotational motion that adheres to the real world, it is mandatory to go beyond the rigid-rotor approximation and include centrifugal distortion ( $\tilde{H}_{04}$ ,  $\tilde{H}_{06}$  and even higher-order terms)<sup>27,28</sup>. In the expression of the centrifugal distortion terms, the opportune power of the rotational angular momentum operator, expressed by the subscript of  $\tilde{H}$ , multiplies the centrifugal distortion constants. Computationally determining these centrifugal distortion constants requires different approximations of the PES entering the Hamiltonian: the harmonic part for the quartics ( $\tilde{H}_{04}$ ) and an anharmonic description for the sextics ( $\tilde{H}_{06}$ ). The tilde sign denotes the result from a Hamiltonian reduction (interested readers are referred elsewhere<sup>27,29</sup>). Note that the Hamiltonian of Eq. 4 applies to the semi-rigid-rotor approximation case (where the term ‘semi-rigid’ implies the treatment of centrifugal distortion) and does not take the effect of molecular vibrations into account. For a more accurate and realistic treatment, the terms describing the vibration–rotation interaction need to be incorporated. These lead to the description of the dependence of the rotational and centrifugal constants on the vibrational quantum numbers.

The interactions of the molecular electric and/or magnetic fields with the nuclear or electron (for open-shell species) moments introduce additional terms into the rotational Hamiltonian<sup>28</sup>, and are responsible for the hyperfine structure in rotational spectra (these aspects are detailed later in the text). It should be noted that some of

these hyperfine interactions are at the basis of magnetic spectroscopies such as NMR<sup>30</sup> and ESR<sup>30,31</sup> for interaction with nuclear and electron magnetic moments, respectively. Although a detailed analysis of those spectroscopies is outside the scope of the present Primer, they play a central role in the study of biological molecules and transition metal complexes in condensed phases<sup>32,33</sup>.

**Vibrational and electronic spectroscopy.** The terms of the vibro-rotational Hamiltonian relevant to vibrational spectroscopy are:

$$\tilde{H}_{\text{vib}} = H_{20} + \tilde{H}_{30} + \tilde{H}_{40} + D \quad (6)$$

where the last term  $D$  incorporates high-order pure vibrational terms as well as those representing the interaction with the rotational motion, such as Coriolis couplings<sup>33,34</sup>. The first term  $H_{20}$  corresponds to the rigid-rotor harmonic-oscillator model, which allows the computation of wavenumbers  $\omega$  and intensities of the fundamental bands based on second derivatives of energy, denoted as quadratic force constants, and first derivatives of properties, such as a dipole moment for infrared spectra or a scalar product of electric and magnetic moment for vibrational circular dichroism (VCD)<sup>35</sup>.

Including only a harmonic description of the PES in the vibro-rotational Hamiltonian results in a simplified description of the vibrational motion. A more realistic picture of the PES requires anharmonic corrections, which complicate the resolution of the corresponding Schrödinger equation. Vibrational perturbation theory to the second order (VPT2)<sup>36,37</sup> offers a very effective solution as the energy levels for all vibrational states can be computed from well-defined combinations of Coriolis couplings together with third and semi-diagonal fourth energy derivatives with respect to normal modes ( $\chi_{ii}$  and  $\chi_{ij}$ ), leading to the anharmonic wavenumbers for fundamentals, overtones and combination bands<sup>38</sup>:

$$\Delta E_i(0-1) = v_i = \omega_i + 2\chi_{ii} + \frac{1}{2} \sum_{i \neq j} \chi_{ij} \quad (7)$$

$$\Delta E_i(0-2) = 2\omega_i + 6\chi_{ii} + \sum_{i \neq j} \chi_{ij} = 2v_i + 2\chi_{ii} \quad (8)$$

$$\Delta E_{ij}(0-1, 0-1)$$

$$= \omega_i + \omega_j + 2\chi_{ii} + 2\chi_{jj} + 2\chi_{ij} + \frac{1}{2} \sum_{k \neq i,j} (\chi_{ik} + \chi_{jk}) \\ = v_i + v_j + \chi_{ij} \quad (9)$$

In a similar manner, anharmonic intensities can be obtained by a double-perturbative approach in which, for both energy and property, the terms beyond the second and first derivatives, respectively, are treated as perturbations, with the unperturbed reference being the harmonic oscillator Hamiltonian. Computationally, this model requires second and semi-diagonal third derivatives of the suitable property, with appropriate equations being available up to three-quanta transitions<sup>35,39–41</sup>.

The most common way to derive the anharmonic PES and property surface for VPT2 computations is based on numerical differentiation of the analytical second

**Normal modes**

Vibrational motion of molecules where all atoms vibrate in phase with the same frequency but with different amplitudes, and the centre of mass remains fixed.

**Overtones**

Vibrational transitions involving the excitation of two or more quanta of a given vibration mode (that is, the quantum number describing the vibrational energy levels change varies by two or more).

**Combination bands**

Observed when two or more vibrations are excited simultaneously.

**Double-perturbative approach**

Simultaneous perturbative treatment of the energy and one property (for example, the electric dipole moment in infrared spectroscopy) around a stationary point.

**Property surface**

(Multidimensional). The variations of a property as a function of suitable nuclear coordinates.

**Large amplitude motions**

Molecular vibrations whose

amplitude is so large that the

harmonic oscillator model is

no longer a reliable zero-order

approximation.

**Density functional theory**  
A quantum-mechanical method in which the properties of a many-electron system are determined using functionals (that is, functions of another function) of the spatially dependent electron density and, possibly, its derivatives.

**Vibrational self-consistent field**

Exploitation of the self-consistent model to treat vibrational motion.

**Vibrational configuration interaction**

Exploitation of the configuration interaction model to treat vibrational motions.

**Vibronic spectroscopy**

Spectroscopy involving the simultaneous excitations of vibrational and electronic states of molecules.

derivatives of the energy and the first derivatives of the properties<sup>34,42,43</sup>. However, energies and/or gradients can also be employed in numerical procedures<sup>42</sup> and, for some electronic structure methods, fully analytical<sup>44,45</sup> derivations have been reported. When taking into account resonance effects and/or decoupled large amplitude motions (LAMs) by reduced-dimensionality variational approaches, the VPT2 model is a very effective workhorse for spectroscopic studies, especially for medium to large-sized molecules<sup>34,35,39</sup>. In addition, vibro-rotational couplings can be written in terms of energy and rotational constant derivatives without any additional electronic energy computation<sup>46</sup>. Effective analytical first and second derivatives of methods rooted into density functional theory (DFT) together with general-purpose vibrational perturbation implementations and reduced dimensionality models now allow for reliable and feasible anharmonic computations of vibrational spectra (such as infrared and Raman) of large systems and also of their chiral counterparts (for example, VCD). Note that semi-diagonal third-energy derivatives with respect to normal modes are also sufficient to evaluate first-order vibrational modulation effects on other spectroscopic parameters such as optical activity, hyperfine tensors and so on.

Alternative methods to perturbative approaches are also possible and include the vibrational self-consistent field<sup>47</sup>, vibrational configuration interaction<sup>48</sup> or vibrational coupled clusters<sup>49</sup>. Despite recent efforts<sup>50</sup>, these methods remain much more difficult to be implemented in generalized ‘black-box’ procedures for non-specialists.

Electronic spectroscopy involves vibrational transitions between different electronic states (see FIG. 1) — and we refer to it as vibronic spectroscopy. Here, vibrational signatures of one-photon absorption and one-photon emission spectra as well as of the chiroptical counterparts (for example, electronic circular dichroism (ECD)) and resonance regimes (resonance Raman) are defined by the overlaps between vibrational wave functions of the initial (*I*) and final (*F*) electronic states ( $\langle \Psi_F(\tau) | \Psi_I(\tau) \rangle$ )<sup>51</sup>. Small amplitude vibrations can be effectively analysed by harmonic models<sup>52,53</sup>, which take into account the difference between the normal modes description in the initial ( $q_I$ ) and final ( $q_F$ ) states using the Shift vector,  $\mathbf{K}$ , and the Duschinsky rotation matrix<sup>54</sup>,  $J$ :

$$q_I = J q_F + \mathbf{K} \quad (10)$$

Strong, bright electronic transitions can be simulated in terms of equilibrium transition dipole moments,  $d_{IF}$ , using the Franck–Condon approach<sup>55,56</sup>. For forbidden or weakly allowed transitions, it is mandatory to include the first derivatives of  $d_{IF}$  with respect to normal coordinates as described by the Herzberg–Teller term<sup>57</sup>:

$$\begin{aligned} & [d_{IF}^{\text{eq}} \langle \Psi_F(\tau) | \Psi_I(\tau) \rangle]^{\text{FC}} \\ & + \left[ \sum_n \frac{\delta d_{IF}^n}{\delta q} \langle \Psi_F(\tau) | \Psi_I(\tau) \rangle \right]^{\text{HT}} \end{aligned} \quad (11)$$

with the sum over  $n$  (in the second term) running over the  $3N - 6$  normal coordinates (which reduces to  $3N - 5$  for linear molecules, with  $N$  being the number of atoms of the molecule). Finally, flexible molecular systems must use internal coordinates, instead of Cartesian

coordinates, whenever curvilinear effects cannot be neglected (as usually occurs with low-frequency modes such as torsions, inversions or ring puckering)<sup>58,59</sup>. In the latter case, the internal coordinate of the decoupled LAM can be treated using a one-dimensional variational model<sup>60</sup>. The considerations above are limited to cases where the Born–Oppenheimer approximation applies. More advanced treatments, including non-adiabatic contributions, are needed for more complex situations such as near conical intersections.

A sketch of the main spectroscopic techniques that can be reliably simulated in this framework is given in FIG. 2, whereas for additional tutorials and reviews see REFS<sup>34,61,62</sup>.

**Chiral spectroscopy.** The chiral spectroscopic techniques addressed in this Primer are limited to optical rotation, ECD and VCD, as well as Raman optical activity (ROA). Optical rotation and ECD are associated with electronic transitions and arise from the differential refraction and absorption, respectively, for left and right circularly polarized light. Optical rotatory dispersion (ORD) is the wavelength dependence of the optical rotation. VCD and ROA are associated with vibrational transitions and arise from the differential absorption and scattering, respectively, for left and right circularly polarized light. The approximations and models related to the vibrational wave functions and their overlaps are the same as those described in the previous section.

ORD is determined by the electric dipole–magnetic dipole polarizability computed using linear response methods implemented in different quantum chemistry software packages<sup>63–65</sup>. Specifically, quantum chemistry programs report the specific rotation at each incident frequency in units of degrees millilitre per gram per decimeter, which can then be directly compared with the experiment. ECD and VCD are determined by the dipole and rotational strengths of electronic or vibrational transitions, respectively, which are related to the scalar products of the electric dipole and magnetic dipole transition moments. For VCD, these are computed using linear response methods at either the harmonic<sup>1,66,67</sup> or anharmonic<sup>35</sup> level. The experiments measure the differential absorbance for left and right circularly polarized light, which is typically converted to the differential molar extinction coefficient  $\Delta\epsilon$  (units of per molarity per centimetre) and is related to the absorbance through Beer’s law<sup>68</sup>. As experimental band shapes of VCD spectra are most frequently Lorentzian whereas the experimental band shapes of ECD spectra tend to be Gaussian, the appropriate line-shape function is employed to convolute the calculated  $\Delta\epsilon$ . For more detail and the relevant conversions, the reader is referred to REFS<sup>1,66,69</sup> for VCD and to REFS<sup>69,70</sup> for ECD.

ROA is determined by electric, magnetic and quadrupole polarizability transition moments of vibrational transitions that are computed using linear response methods at either the harmonic<sup>67,71,72</sup> or anharmonic<sup>35</sup> level. In the far from resonance theory, where the exciting laser radiation is far from the lowest allowed electronic excited state, ROA intensity differences are determined by three tensor invariants constructed as linear combinations of products of these polarizability

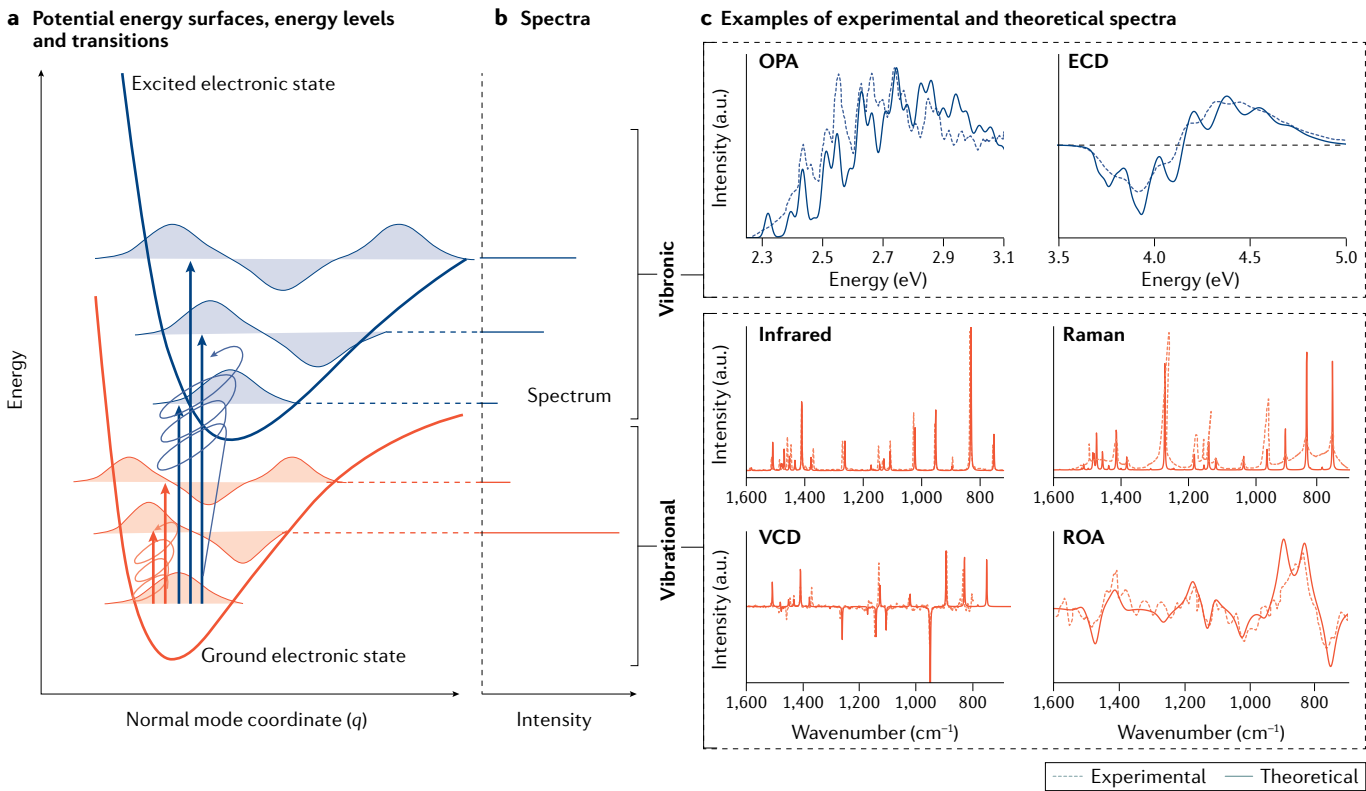


**Fig. 2 | General theoretical framework for vibrational and vibronic spectroscopies and their chiral counterparts.**  
**a** | Schematic of the ground (orange) and excited (blue) electronic state potential energy surfaces (PESs), vibrational energy levels and wave functions. The energy scale underestimates the gap between the two electronic states. Straight arrows represent transitions from the vibrational ground state: vibrational (orange: infrared and Raman) and vibronic (involving both states; blue: one-photon absorption (OPA)). Circled arrows represent the interaction with circularly polarized light corresponding to vibrational circular dichroism (VCD; orange), Raman optical activity (ROA; orange) and electronic circular dichroism (ECD; blue) spectroscopies. **b** | Schematic of resulting vibrational and vibronic line positions and corresponding intensities. **c** | Examples of simulated and experimental spectra from REFS<sup>17,35</sup>. OPA and ECD spectra in part **c** adapted with permission from REF.<sup>259</sup>, Royal Society of Chemistry. Infrared, Raman, VCD and ROA spectra in part **c** adapted with permission from REF.<sup>35</sup>, American Chemical Society.

**One-photon absorption**  
A spectroscopic technique in which one-photon absorption leads from the electronic ground state to an excited electronic state.

**One-photon emission**  
A spectroscopic technique in which one-photon emission leads from an excited electronic state to a less-excited (lower energy, usually the ground) state.

**Electronic circular dichroism**  
Electronic version of circular dichroism.

**Optical rotation**  
The rotation angle of the polarization plane of polarized light issuing from its passage through a layer or a liquid, determined by the concentration of chiral molecules and their structure in a substance.

tensors<sup>1,69,73,74</sup>. There are several different forms of ROA that depend upon the choice of polarization modulation and scattering geometry, although the most common is backscattered circular polarization denoted SCP(180). Quantum chemistry programs report the ROA scattering activities for a specific experimental set-up, which are then converted into a differential scattering cross-section including a factor of  $(\nu_{\text{inc}} - \nu_i)^4$ , where  $\nu_{\text{inc}}$  and  $\nu_i$  are the wavenumbers for the incident frequency and mode  $i$ , respectively<sup>69,75,76</sup>. As experimental band shapes are typically Lorentzian, calculated spectra are plotted using the Lorentzian line-shape function. As absolute ROA intensities are not typically measured, it is common practice to label the intensity differences as  $I_R - I_L$ , as is done for the experimental spectra.

**Diffusion Monte Carlo.** An alternative to conventional time-independent computational approaches to rotational and vibrational spectroscopy is offered by the imaginary-time propagation of the time-dependent Schrödinger equation:

$$|\Psi(\tau)\rangle = \sum_n c_n e^{-\tau(E_n - V_{\text{ref}})} |\phi_n\rangle \quad (12)$$

where  $|\phi_n\rangle$  is an eigenstate of the Hamiltonian, with energy  $E_n$ <sup>77–86</sup> and  $\tau = it/\hbar$ . When we propagate an arbitrary wave function in imaginary time, at long times the leading contribution to the wave function will be the ground state. Further, if  $V_{\text{ref}} = E_0$ , the amplitude of the wave function will remain constant. The advantage of DMC approaches over conventional approaches comes in the representation of the wave function. In the simplest implementation of DMC,  $|\Psi(\tau)\rangle$  is represented by an ensemble of localized functions  $g(\mathbf{x} - \mathbf{x}_i)$ :

$$\langle \mathbf{x} | \Psi(\tau) \rangle = \sum_i w_i(\tau) g(\mathbf{x} - \mathbf{x}_i) \quad (13)$$

At each time step in the simulation, each of the components of each of the  $\mathbf{x}_i$  values is displaced by a random value based on Gauss random distributions, where the distribution for the  $j$ th atom has a width of  $\sqrt{\frac{\Delta\tau}{m_j}}$ , where  $m_j$  represents the corresponding mass. After the atoms are displaced, the potential energy is evaluated, and the weight  $w_i(\tau)$  is adjusted according to:

$$w_i(\tau + \Delta\tau) = e^{(V(\mathbf{x}_i) - V_{\text{ref}})\Delta\tau} w_i(\tau) \quad (14)$$

**Raman optical activity**  
Vibrational spectroscopy based on the differential Raman scattering of left and right circularly polarized light due to molecular chirality.

**Optical rotatory dispersion**  
The variation of the optical rotation of a substance with a change in the wavelength of light.

**Line-shape function**  
A mathematical function (usually Gaussian, Lorentzian or a combination of both) describing phenomenologically the shape of a spectral band.

**Imaginary-time**  
Time rotated into the imaginary plane via Wick rotation in DMC,  $\tau = it/\hbar$ .

This relatively simple algorithm provides a Monte Carlo sampling of the ground-state wave function for the molecule of interest based on the provided potential surface as well as the ground-state energy. By propagating the ensemble forwards in time we can obtain the information required to generate the ground-state probability amplitude<sup>84,87</sup>. Such information allows us to explore how the molecule samples the potential and evaluate, for example, rotational constants for obtaining rotational spectra. Finally, energies and wave functions for rotation or vibrationally excited states can be obtained using this approach by imposing a nodal structure for these

states<sup>86,88,89</sup>. The major advantage of DMC over more conventional approaches is that it allows a way to explore the role of nuclear quantum effects in systems where the ground-state wave function is delocalized among multiple local minima on the potential surface. These are situations where approaches such as perturbation theory become less effective.

### Software for computational spectroscopy

Some available quantum chemistry packages together with their potentialities and main features are provided in TABLE 1.

**Table 1 | Common software packages for computational spectroscopy applications with their quantum chemistry methodologies and main spectroscopic features**

Software package	Methodology	Spectroscopic applications
<a href="#">CFOUR</a> (academic)	CC theory/MP2 (Analytic second derivatives)	Rotational spectroscopy: all parameters Vibrational spectroscopy: VPT2
	CC composite schemes	NMR/ESR spectroscopies: all parameters
<a href="#">Gaussian</a> (commercial)	DFT/TD-DFT/MP2 (Analytic Hessians)	Rotational spectroscopy: all parameters Vibrational spectroscopy: infrared, Raman, VCD, ROA
	CCSD(T) energies	Electronic spectroscopy: UV–Vis, ECD, RR, RROA
	QM/QM'/MM/PCM	NMR/ESR spectroscopies: all parameters
<a href="#">Molpro</a> (commercial)	CC and explicitly correlated CC	Rotational spectroscopy: equilibrium rotational constants
	Multi-reference methods	Vibrational spectroscopy: VSCF/VCI
	DFT/TD-DFT	
<a href="#">NWChem</a> (academic)	CC theory energies	Rotational spectroscopy: equilibrium rotational constants
	MP2 analytical gradients	Vibrational spectroscopy: VSCF energies
	DFT/TD-DFT	Electronic spectroscopy: UV–Vis
	QM/MM	NMR: shielding tensors and indirect spin–spin coupling
	COSMO/SMD/VEM	
<a href="#">ORCA</a> (academic)	CC and explicitly correlated CC	Rotational spectroscopy: equilibrium rotational constants
<a href="#">ORCA</a> (commercial)	Local correlation methods	Vibrational spectroscopy: infrared, Raman, RR, NRVS
	Multi-reference methods	Electronic spectroscopy: UV–Vis, ECD, MCD, fluorescence, phosphorescence, band shapes
	DFT/TD-DFT	NMR/ESR spectroscopies: all parameters
	QM/MM, embedding schemes	X-ray absorption/emission, RIXS, Mössbauer
	Implicit solvation	
<a href="#">QChem</a> (commercial)	CC theory (ground and excited states, spin-flip methods), MP2/ADC schemes (energies and gradients)	Rotational spectroscopy: equilibrium rotational constants
	DFT/TD-DFT	Vibrational spectroscopy: infrared/Raman, anharmonic energies TOSH, VPT2, VCI
	QM/MM	Electronic spectroscopy: UV–Vis, RR
	PCM	
<a href="#">PSI4</a> (academic)	CC/MP2	Spectroscopic constants for diatomics from PES fit
	CCSD(T) gradients	Rotational spectroscopy: equilibrium rotational constants
	CC/MP2 composite schemes for energies, gradients and Hessians	Vibrational spectroscopy: harmonic models
	DFT/TD-DFT	Electronic spectroscopy: UV–Vis, OR
	Solvent via external codes	

ADC, algebraic diagrammatic construction; CC, coupled-cluster; CCSD(T), coupled-cluster theory with single and double excitations and perturbative treatment for triple excitations; COSMO, COnductor like Screening MOdel; ECD, electronic circular dichroism; ESR, electron spin resonance; MCD, magnetic circular dichroism; MM, molecular mechanics; MP2, Møller–Plesset theory; NMR, nuclear magnetic resonance; NRVS, nuclear resonance vibrational spectroscopy; OR, optical rotation; PCM, polarizable continuum model; PES, potential energy surface; QM, quantum mechanics (QM', a different QM level); RIXS, resonant inelastic x-ray scattering; ROA, Raman optical activity; RR, resonance Raman; RROA, resonance Raman optical activity; SMD, solvent model based on density; (TD)-DFT, (time dependent)-density functional theory; TOSH, Transition Optimized Shifted Hermite; VCD, vibrational circular dichroism; VCI, vibrational configuration interaction; VEM, vertical excitation model; VPT2, vibrational perturbation theory to the second order; VSCF, vibrational self-consistent field.

**Coupled-cluster theory**  
A hierarchy of electron correlation methods that, by means of an exponential Ansatz, systematically converge to the exact solution of the molecular Schrödinger equation starting from the independent particle Hartree–Fock model.

#### CCSD(T)

A coupled-cluster method that considers full account of single and double excitations and a perturbative treatment of triple excitations.

#### Electron correlation

The effects of electron–electron interactions beyond the mean field Hartree–Fock model.

#### Domain-based pair natural orbitals

Electron pair-specific localized natural orbitals expanded in a set of local atomic orbitals belonging to pair-specific domains.

#### Global-hybrid or double-hybrid density functionals

Families of density functionals including a percentage of Hartree–Fock exchange (hybrid) and MP2-type correlation (only double-hybrid).

#### Møller–Plesset theory to the second order

Møller–Plesset theory including many-body effects on top of the mean field Hartree–Fock reference wave function up to the second order of perturbation theory.

#### Equation of motion

In a quantum chemistry context, a methodology for treatment of electronically excited or ionized states.

#### Density matrix renormalization group

A very efficient numerical variational technique devised to obtain the lowest-energy wave function of a given Hamiltonian expressed in terms of a matrix product state.

#### CASPT2

A specific generalization of Møller–Plesset theory to the second order to multiconfigurational reference wave functions.

#### NEVPT2

A variant of second-order multi-reference perturbation theory similar to CASPT2.

## Computational requirements

The computational requirements strongly depend on the type of spectroscopic technique under consideration and the specific accuracy required.

For rotational spectroscopy, the principal properties to accurately compute are the equilibrium rotational constants, which are derived from equilibrium structure determinations, whereas for vibrational spectroscopy they are the harmonic frequencies from harmonic force-field evaluations. To obtain accurate results, errors in the electronic structure calculations due to the truncation of both the basis set (one-electron error) and the wave function ( $N$ -electron error) must be minimized. To achieve this goal, composite schemes evaluate the contributions important to reach the best possible accuracy and then combine them through the additivity approximation (see, for example, REFS<sup>90–102</sup>). These composite schemes usually involve the coupled-cluster (CC) theory<sup>103</sup> and, in particular, the coupled-cluster single and double excitations and a perturbative treatment of triples (CCSD(T)) method<sup>104</sup>, which is often denoted as the ‘gold standard’ for accurate calculations and thus for incorporating most of the dynamic electron correlation. On the other hand, the introduction of explicitly correlated (F12) treatments<sup>105</sup> can partially recover the one-electron error without extrapolation techniques. The development of local correlation treatments based on domain-based pair natural orbitals<sup>106,107</sup> allows, instead, for improving the scaling of coupled-cluster treatments with the number of electrons.

From a computational point of view, going beyond the rigid-rotor harmonic-oscillator approximation increases the complexity and the cost of electronic structure calculations. The level of theory for the electronic computations must therefore be reduced and approximations for the solution of the nuclear problem introduced. Global-hybrid or double-hybrid density functionals<sup>108–110</sup> provide an optimal alternative to low-cost ab initio electronic computation methodologies such as the Møller–Plesset theory to the second order (MP2)<sup>111</sup>, whereas VPT2 offers a powerful tool to approximate the nuclear problem solution. Hybrid coupled-cluster/DFT models, employing anharmonic corrections and/or property predictions beyond the electric dipole moment from DFT, represent nearly optimal compromises between feasibility and accuracy<sup>35,112,113</sup>.

Applying DFT approaches to computational spectroscopy studies requires careful benchmarking of all the required properties such as equilibrium structures, harmonic and anharmonic frequencies, and property derivatives. Unfortunately, most of the benchmark studies reported to date have focused on the accuracy of energetic properties for selected equilibrium structures<sup>114–117</sup>, with conclusions that cannot be directly generalized to assess the accuracy of wider regions of the PES or other properties<sup>62,118–120</sup>. Flexible systems such as most biomolecules have flat PESs whose behaviour cannot be described in terms of the well-separated energy minima within nearly-harmonic basins that have been considered in most benchmarks. Concerning other properties, the interpretation of important spectroscopic techniques requires computed properties that have not yet been validated in a

comprehensive way. Only a limited number of functionals and basis sets have been benchmarked for geometric structures<sup>120–126</sup>, anharmonic vibrational frequencies<sup>62,118,119,126,127</sup> and other spectroscopic properties<sup>119,126</sup>. In addition, second and higher analytical derivatives of energy and properties are often not implemented in some of DFT models, which hampers their application. For excited electronic states, the first benchmark studies going beyond vertical excitation energies have been recently reported<sup>128,129</sup>, whereas the implementation of analytical time-dependent DFT Hessians allows more efficient VPT2 computations for excited electronic states of medium to large-sized molecules<sup>130</sup>. A more reliable but much more computationally expensive alternative to DFT is offered by highly accurate equation of motion (EOM) coupled-cluster methods<sup>131</sup>. Despite the successful applications of DFT and single-reference many-body approaches, multi-reference methods<sup>132</sup> based on wave functions described by linear combinations of several electronic configurations cannot be avoided whenever (non-dynamic) static electron correlation is important, as they can successfully address strong correlation effects. We also note that modern linear or low-order scaling local correlation methods based on MP2 or CCSD(T) have found increasing use in quantum chemistry and theoretical spectroscopy<sup>133–135</sup>. However, a more detailed description of these aspects is outside the scope of this Primer.

The most generally applicable methods in transition-element theoretical spectroscopy are based on traditional<sup>18</sup> or more recent (for example, density matrix renormalization group<sup>136</sup>) multi-reference wave function-based theories. These methods can now be routinely applied to larger molecules (100–200 atoms). Although they have been used extensively in the form of, for example, CASPT2 (complete active space perturbation theory to the second order)<sup>137,138</sup> or NEVPT2 ( $N$ -electron valence state perturbation theory to the second order)<sup>139</sup>, severe limitations still exist that will provide incentive for method developers for decades to come. A more thorough description of these approaches and their strengths and weaknesses is outside the scope of this Primer.

TABLE 2 provides a non-exhaustive summary of the computational evaluation of spectroscopic parameters where we collect, for each spectroscopic technique considered in this Primer, the best accuracy obtainable, the type of computation required, the level of theory and the affordable dimension of the system. Note that this table is based on analytical derivative techniques, which means that there can be further extensions in terms of properties and levels of theory.

## Results

In this section, we select a few spectroscopic techniques to provide examples of how to process, treat and interpret spectroscopic data for spectroscopies involving rotational and vibrational motions.

### Rotational spectroscopy for structure

Despite the fact that rotational spectroscopy is the technique of choice for determining accurate molecular structures, such derivations are seldom straightforward. Extracting geometrical parameters from the experimental

Table 2 | Quantum chemistry methodologies (and expected accuracy) for the evaluation of spectroscopic parameters

Spectroscopy	Spectroscopic parameters	Accuracy	Quantum chemistry calculations	Quantum chemistry methodology and feasible number of atoms	
				Wave function	DFT
Magnetic	Chemical Shifts	Moderate; variable for different nuclei	Response property calculation for imaginary and triplet perturbations	CCSD(T)<10	GGA <2,000
	Spin–spin coupling			Local CCSD(T)<200	Hybrid <1,000
	<i>g</i> -Tensor			(Local) MP2 <200	Double-hybrid <100
	Zero-field splitting			HF<1,000	
	Hyperfine coupling				
	Quadrupole coupling				
Nuclear	Mössbauer	10 <sup>-9</sup> eV	Isomer shift, quadrupole splittings, low-energy vibrational modes	CCSD <10 DLPNP-CCSD <100	DFT <1,000
	NRVS	<10%		CCSD <10 DLPNO-MP2 <200	
	Rotational constant: equilibrium	<0.1% to 0.5%	Geometry optimization (minimum of the PES)	Composite schemes <30	Hybrid >100 Double-hybrid <100
	Rotational constant: vibrationally averaged	0.1–2%	Anharmonic force field (second and third energy derivatives)	MP2 <20 CCSD(T)<10	Hybrid <100 Double-hybrid <20
Rotational	Centrifugal (quartic) distortion constants	<1%	Harmonic force field	Composite schemes <15	Hybrid <30 Double-hybrid <20
	Vibrational frequency: harmonic	1–20 cm <sup>-1</sup>	Harmonic force field	Composite schemes <15	Hybrid <400 Double-hybrid <50
	Vibrational frequency: anharmonic (VSCF/VCI/VPT2)	1–10 cm <sup>-1</sup>	Anharmonic contributions (third and fourth energy derivatives)	MP2 <20 CCSD(T)<10	Hybrid <50 Double-hybrid <20
	Infrared/Raman intensities: harmonic	10 km mol <sup>-1</sup>	Dipole moment/polarizability: first derivative with respect to nuclear coordinate	Composite schemes <15	Hybrid <100 Double-hybrid <50
	Infrared/Raman intensities: anharmonic	5 km mol <sup>-1</sup>	Dipole moment/polarizability: second/third derivative with respect to nuclear coordinate	MP2 <20 CCSD(T)<10	Hybrid <50 Double hybrid <20
	VCD/ROA intensities: harmonic	10–30%	Magnetic moments: first derivative with respect to nuclear coordinate	CCSD <15 (ROA only)	Hybrid <100
Vibronic	VCD/ROA intensities: anharmonic		Magnetic moments: second/third derivative with respect to nuclear coordinate	–	Hybrid <50
	Electronic energy	0.1–0.5 eV	Initial–final state energy difference between	MRCI, ADC EOM-CCSD <50 DLPNO-STEOM-CCSD <150	TD-DFT <200 TDA <2000
	Ground-state equilibrium structure, normal modes and frequencies	(see rotational and vibrational)			
	Excited electronic state equilibrium structure	0.02–0.1 Å	Geometry optimization (minimum of the PES)	ADC(2)<50 EOM-CCSD, CC3 <15	TD-DFT <100 TDA <200
	Excited electronic state normal modes and harmonic frequencies	30 cm <sup>-1</sup>	Harmonic force field (analytical or numerical differentiation of analytical gradient)	EOM-CCSD <20	TD-DFT <100 TDA <200
	Excited electronic state normal modes and anharmonic frequencies	10 cm <sup>-1</sup>	Anharmonic contributions (third and semi-diagonal fourth derivative)	MRCI, EOM-CCSD <6	TD-DFT <20
	OPA/OPE/ECD	0.2 eV	Electric and/or magnetic transition moment	EOM-CCSD, CC3 <15	TD-DFT <100 TDA <200
	FC/HT	0.05 eV	Transition moment derivatives	EOM-CCSD <15	TD-DFT <100

Table 2 (cont.) | Quantum chemistry methodologies (and expected accuracy) for the evaluation of spectroscopic parameters

Spectroscopy	Spectroscopic parameters	Accuracy	Quantum chemistry calculations	Quantum chemistry methodology and feasible number of atoms
				Wave function DFT
X-ray	K-edge absorption	1 eV	Excitation energies	EOM-CCSD <20
	L-edge absorption	10% relative intensity	Multipole transition moments	MRCI <10
	K-β emission			NEVPT2 <200
	RIXS			CIS <1,000

ADC, algebraic diagrammatic construction; CC3, approximate coupled cluster singles, doubles, and triples model; CCSD(T), coupled-cluster theory with single and double excitations and perturbative treatment for triple excitations; CIS, configuration interaction singles; DFT, density functional theory; ECD, electronic circular dichroism; EOM, equation of motion; FC/HT, Franck–Condon/Herzberg–Teller; GGA, generalized gradient approximation; MP2, Moller–Plesset theory; MRCI, multi-reference configuration interaction; NEVPT2, N-electron valence state perturbation theory to second-order; NRVS, nuclear resonance vibrational spectroscopy; OPA, one-photon absorption; OPE, one-photon emission; PES, potential energy surface; RIXS, resonant inelastic x-ray scattering; STEOM, similarity transformed equations of motion; TD, time dependent; TDA, Tamm–Dancoff approximation; VCD, vibrational circular dichroism; VCI, vibrational configuration interaction; VPT2, vibrational perturbation theory to the second order; VSCF, vibrational self-consistent field.

information (that is, the rotational constants) is hampered by the number of data actually available (that is, the number of rotational constants for different isotopic species) and vibrational effects<sup>6</sup>. These difficulties can be overcome by the fruitful interplay of high-resolution spectroscopy and quantum chemistry via the so-called semi-experimental approach, illustrated in FIG. 3.

The semi-experimental approach leads to equilibrium structures — by definition, the geometries corresponding to minima on the PES — by least squares-fitting the structural parameters to the semi-experimental equilibrium rotational constants ( $B_{i,e}^{\text{SE}}$ ).  $B_{i,e}^{\text{SE}}$  terms are determined by subtracting the computed vibrational corrections ( $\Delta B_{i,0}^{\text{calc}}$ ) from the experimental vibrational ground-state rotational constants ( $B_{i,0}^{\text{exp}}$ )<sup>6</sup>:

$$B_{i,e}^{\text{SE}} = B_{i,0}^{\text{exp}} - \Delta B_{i,0}^{\text{calc}} = B_{i,0}^{\text{exp}} + \frac{1}{2} \sum_n \alpha_i^n \quad (15)$$

where  $i$  denotes the principal inertial axis ( $a$ ,  $b$  or  $c$ ; so that  $B_{i=a} = A$ ),  $\alpha_i^n$  are the vibration–rotation interaction constants and the sum is taken over all fundamental vibrational modes  $n$ <sup>28</sup>. Equation 15 shows that vibrational effects are removed from the treatment via subtraction of the corresponding corrections. To overcome the limited number of experimental information (for a given isotopologue, there are at most three rotational constants), we consider different isotopic species. These isotopic species share the same equilibrium structure (because the PES of a given molecule is isotope-independent within the Born–Oppenheimer approximation) but have different equilibrium rotational constants (because equilibrium rotational constants also depend on the isotopic masses), thus increasing the amount of experimental data. A sufficient number of isotopic species is required to provide enough information for complete structural determination such that there are more data than geometrical parameters. Vice versa, high-level quantum chemistry calculations can accurately predict the rotational parameters<sup>140</sup> to be used to plan, guide and interpret experiments<sup>34</sup>. The interplay shown in FIG. 3 can be enhanced by exploiting graphical tools to visualize, compare and manipulate spectra as well as handle their assignment<sup>141</sup>.

Although the success of the semi-experimental approach in FIG. 3 is well-established for small to

medium-sized semi-rigid molecules, the situation is more complex for larger and usually less rigid molecular systems. In recent years, laser ablation vaporization<sup>142</sup> and broadband<sup>9</sup> techniques have shifted the targets of spectroscopic studies towards flexible molecules and non-covalent molecular complexes involving more than two molecules. Both categories are usually characterized by a large number of closely spaced energy minima (broadly referred to as conformers or isomers) that all contribute to the overall spectrum. A correct spectral analysis therefore requires knowledge of the rotational spectra of all isomers and/or conformers present in the gas-phase mixture. The overall rotational spectrum is then obtained by weighting each contribution according to its isomer and/or conformer population. Therefore, an incomplete account of conformers can easily generate unsatisfactory modelling in a similar way to wrong equilibrium structure determination when considering a semi-rigid molecule. Overcoming these difficulties requires powerful unsupervised techniques, such as machine learning algorithms, to explore the degrees of freedom associated with the LAMs<sup>143</sup>.

### Vibrational effects in flexible systems

The simplest approach to vibrational spectroscopy is based on the double harmonic approximation, which employs quadratic and linear approximations for the PES (for transition frequency) and property surface (for intensity), respectively. This tool is available in several electronic structure quantum mechanics codes and becomes extremely efficient whenever analytical energy second derivatives and property gradients are available. Mechanical (PES) and electric/magnetic (property surface) anharmonicities can be introduced by means of perturbative<sup>34,35,39–41,43</sup> or variational<sup>34,47,48,144–146</sup> time-independent approaches. Despite some limitations such as, for example, the treatment of LAMs, perturbative time-independent approaches can robustly simulate spectral line shapes, thereby allowing vis-à-vis comparison with experimental outcomes<sup>35,39–41,61</sup>. Simultaneously integrating both models within a general platform allows the correct treatment of small amplitude motions and LAMs<sup>142</sup>. Dedicated graphical tools such as the Virtual Multifrequency Spectrometer (VMS)<sup>61</sup> greatly facilitate spectral simulation, analysis and comparison with experiments.

**CIS**  
Configuration interaction  
(that is, mixing of ground and excited electronic states)  
including only single excitations from a reference Slater determinant.

**Multi-reference configuration interaction**  
Extension of the configuration interaction approach to multi-reference wave functions.

**Tamm–Dancoff approximation**  
From a practical point of view, a synonym of CIS.

**Isotopologue**  
Isotopic species of a molecule.

**Harmonic approximation**  
A model in which the vibrational motion is described in terms of masses attached to a spring, whose energy is governed by a quadratic potential.

**Small amplitude motions**  
Molecular vibrations whose amplitude is small enough that the harmonic oscillator is a reliable zero-order approximation.

**Innocent solvents**

Solvents that do not establish specific interactions, for example, hydrogen bonds with the solute.

**Polarizable continuum model**

A description of bulk solvent effects in terms of a polarizable continuum in which the solute is fully embedded.

**Cybotactic region**

The region around a solute molecule including solvent molecules belonging to the first solvation shell, that is, showing close solute–solvent contacts.

**0–0 transition**

The transition between the vibrational ground states of initial and final electronic states.

Time-independent models employ structures and properties of energy minima and their local environments in variational or perturbative formalisms mostly exploiting the Watson Hamiltonian<sup>34</sup> (given in Eq. 3 and discussed in Experimentation). By contrast, time-dependent approaches perform classical or semi-classical dynamics simulations over the whole PES and the corresponding property surface<sup>147–149</sup>. The two approaches (time-independent and time-dependent) offer complementary information and selecting the most appropriate strategy depends on several factors including the environment (for example, time-independent models are more suitable for isolated molecules and time-dependent ones for condensed phases), the effective mass governing the motion (for example, classical time-dependent models are more effective for large masses) and other effects. Flexible molecular systems should use harmonic models based on curvilinear coordinates<sup>58</sup>; for systems with several low-lying conformers/tautomers, appropriate averaging of individual spectra must be performed. As in rotational spectroscopy, the presence of several low-lying conformers/tautomers can tune the overall spectrum and requires appropriate conformational searches and weighting of the spectra of the most stable structures by the corresponding Boltzmann populations<sup>150</sup>. For solutions, the solvatochromic effects in innocent solvents can be incorporated at a negligible cost by using the polarizable continuum model<sup>34</sup>. In more complex cases, the solvent molecules in the cybotactic region must be explicitly included<sup>151</sup> at the very least.

In electronic spectroscopy, absorption or emission spectra represent the envelopes of transitions between specific vibrational levels of the initial and final electronic states. However, most current computations still employ rough phenomenological models where empirical Gaussian or Lorentzian functions broaden vertical transition energies. In addition, the analysis of experimental data is often based on the assumption that the peak maxima are related to the 0–0 transition, even though it is impossible to know *a priori* which vibronic transition will be most intense as this depends on the largest overlap of vibrational wave functions. Therefore, realistic simulations must take into account vibrational effects. In the Franck–Condon approximation, the transition dipole moment (Eq. 11) is considered constant and nuclear coordinate-independent in harmonic time-independent (sum of state)<sup>52</sup> or time-dependent (path integral)<sup>53</sup> approaches. The simplest formulation of vibrational modulation effects is therefore based on one-dimensional vibrational overlaps between identical normal modes of the different electronic states (with the possibility of reducing the number of identical normal modes). This approach is still employed and is also exploited in the prescreening procedure for more sophisticated time-independent computations<sup>51</sup>. More accurate direct nuclear dynamics simulations are prohibitive for large systems and, as such, the most advanced models employing highly accurate PESs and property surfaces can only be applied to small-sized molecules<sup>144–146</sup>. Integration of time-independent and time-dependent models within a general platform allows both simulation

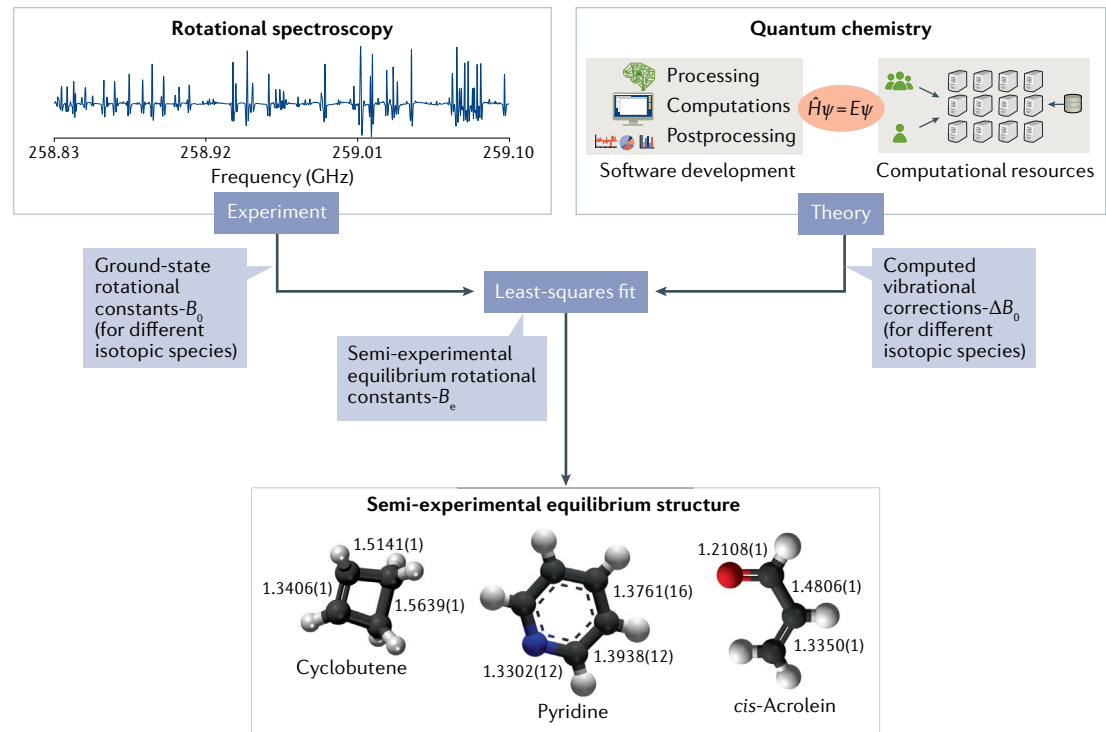


**Fig. 3 | Schematic interplay of experiment and theory in rotational spectroscopy to determine equilibrium structure.** Experimental vibrational ground-state rotational constants are computationally corrected for vibrational effects. The resulting semi-experimental equilibrium rotational constants for different isotopic species allow for the determination of the equilibrium structure.

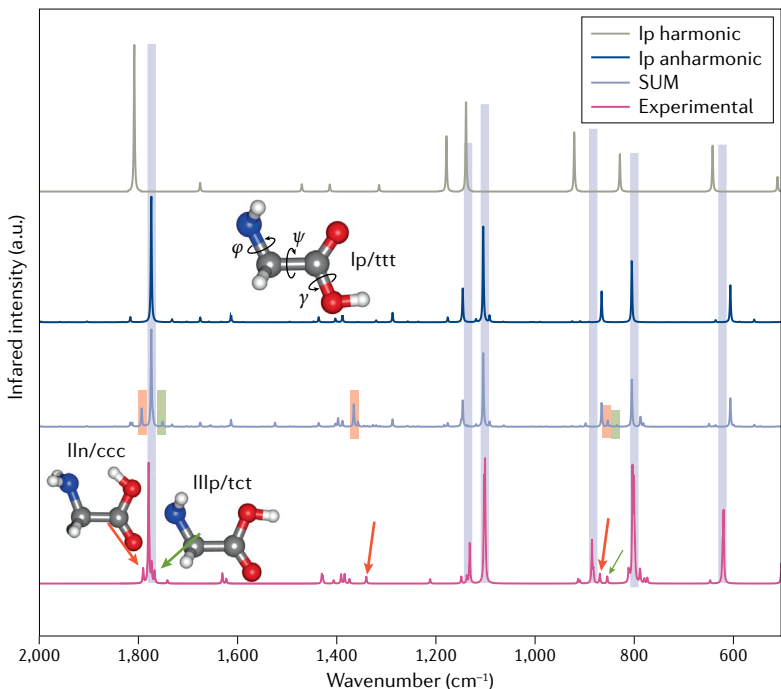


**Fig. 4 | Computed<sup>113</sup> and experimental<sup>157</sup> matrix-isolation infrared spectra of glycine.** Simulated harmonic and anharmonic theoretical spectrum of the most stable Ip conformer together with the final spectrum resulting from the sum of the contributions of Ip/ttt, IIln/ccc and IIIlp/tct conformers, weighted for their relative abundances, at 410 K (temperature of the sample preparation), also assuming the conformational cooling of less stable conformers. The contributions from the three conformers to the ‘SUM’ spectrum are highlighted by coloured regions and/or arrows (Ip, blue; IIln, red; IIIlp, green). c, cis orientation; n, non-planarity of the backbone; p, planarity of the backbone; t, trans orientation. Computed spectra adapted with permission from REF.<sup>113</sup>, Royal Society of Chemistry. Experimental spectra adapted with permission from REF.<sup>157</sup>, American Chemical Society.

of highly resolved spectra (including band assignments) and full convergence of spectra at finite temperatures. For more complex and flexible systems, several approximate yet sufficiently accurate approaches have been proposed<sup>34,152–154</sup> for both vibrational and vibrationally resolved electronic spectra.

**The matrix-isolation infrared spectrum of glycine.** A step-by-step route from the starting harmonic computations to the final realistic simulated spectra is presented in FIG. 4 for glycine ( $\text{H}_2\text{NCH}_2\text{COOH}$ ), the simplest amino acid. Glycine is characterized by conformational flexibility due to rotation along three single bonds: N–C, C–C and C–O. The small size of the molecule allows for a full theoretical exploration of its conformational space, confirming the presence of eight local minima<sup>113,120,155</sup> labelled by roman numbers (I–VIII, with the lowest number denoting the most stable conformer), with ‘p, n’ describing the planarity or non-planarity of the backbone and ‘c, g, t’ the *cis*, *gauche* or *trans* orientation of the lone pair (N)–N–C–C, N–C–C–O and C–C–O–H dihedrals.

The six most stable glycine conformers have been studied using Fourier transform infrared spectroscopy, with three conformers detected under the same experimental conditions<sup>156–158</sup>. FIGURE 4 compares computed spectra with Fourier transform infrared results

for glycine deposited in a low-temperature matrix. The harmonic spectrum of the most stable conformer Ip identifies the most intense experimental bands. An improved and more realistic spectrum is obtained by including anharmonic corrections to band positions and intensities, resulting in the appearance of several new bands related to non-fundamental transitions. Fully anharmonic computations permit one to disentangle low-intensity bands related to overtones and/or combination bands of the most abundant conformer (not present at the harmonic level) from fundamental transitions of the less abundant ones (see REF.<sup>113</sup> for detailed discussion and analysis). The best agreement with experiment is obtained once the contributions from the IIln and IIIlp conformers, weighted for their Boltzmann populations, are added.

**Vibronic spectrum of chlorophyll a.** Vibronic spectra simulations are necessary to disentangle the different contributions to the overall line shape, especially in the presence of different electronic transitions, conformers or additional species possibly present in the experimental mixture (for instance, photoproducts<sup>159</sup>). In FIG. 5, the simulated UV–Vis spectrum of chlorophyll *a* in methanol solution is compared with the experimental counterpart. Environmental effects are taken into account using a hybrid implicit/explicit solvent model with the two methanol molecules coordinating the magnesium ion and the bulk solvent effects accounted for using the polarizable continuum model (see REF.<sup>160</sup> for the details, and REF.<sup>135</sup> for the gas-phase spectrum simulation).

The spectra of chlorophylls are traditionally described in terms of four bands based on the simplified four-orbital Gouterman model<sup>161</sup>, with two low-energy Q bands and two high-energy B bands. In the present case, the additional *x/y* labelling can be used, depending on the transition moment polarization within the macrocycle plane<sup>162</sup>. FIGURE 5a demonstrates how the set of vibronic transitions defines the asymmetrical shape of the lowest energy  $S_1 \leftarrow S_0$  transition, which cannot be well described by the simplest vertical energy approach irrespective of the applied broadening. This transition dominates the  $Q_y$  band and significantly contributes to the  $Q_x$  band. In FIG. 5b, the final spectrum obtained from the contributions of the individual  $S_x \leftarrow S_0$  ( $x = 1–8$ ) transitions can be directly compared with the experimental spectrum in the whole UV–Vis range. Simulation of vibronic spectra allows for the unequivocal assignment of the main spectral features, showing that the line shape is dominated by two pairs of overlapping transitions:  $S_1 \leftarrow S_0$  and  $S_2 \leftarrow S_0$  being the first pair and  $S_3 \leftarrow S_0$ ,  $S_4 \leftarrow S_0$  the second. These pairs give rise to the  $Q_y/Q_x$  and  $B_y/B_x$  bands, respectively.

#### Molecular vibrations from DMC

Insights into molecules that undergo large amplitude vibrations can be obtained from how the ground-state wave function samples the potential surface, and how this is affected by isotopic substitution. DMC provides an approach that is well suited to exploring the ground-state properties of molecules showing LAMs. The power of the DMC approach comes from the representation

Half-width at half-maximum  
Half of the width between the two points where the value of the function is its half-maximum.

#### Zero-point energy

The lowest energy that a quantum system may have, which, contrary to the classical case, is non-zero due to the Heisenberg uncertainty principle.

#### Ensemble of walkers

A large number of virtual copies of a single particle moving randomly over a given potential energy surface.

of the wave function by an ensemble of localized functions (or walkers) as described by Eq. 12, which allows the study of systems that are not well approximated by a simple zero-order harmonic description such as, for example, torsions around simple bonds or ring puckerrings. The downside of the DMC approach is that, generally, only one state can be calculated at a time, making it well-suited for studies that focus on the ground-state wave function and associated properties, including vibrationally averaged rotational constants.

To obtain state energies from DMC, the reference energy<sup>86</sup> is evaluated at each time step  $\tau$  in the DMC propagation:

$$V_{\text{ref}} = \bar{V}(\tau) - \alpha \left( \frac{N_w(\tau) - N_w(0)}{N_w(0)} \right) \quad (16)$$

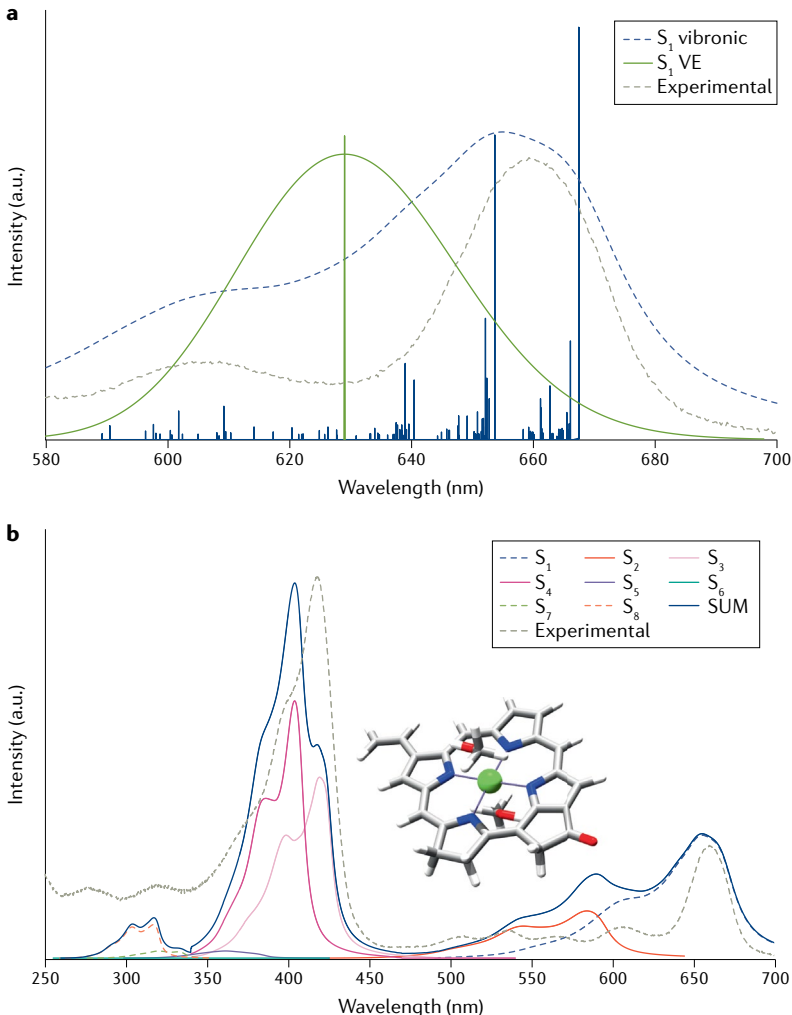


**Fig. 5 | Computed<sup>160</sup> and experimental<sup>160</sup> UV-Vis spectrum of chlorophyll a in methanol.** Simulated theoretical spectra. **a** |  $S_1 \leftarrow S_0 (Q_y)$  transition simulated by the vertical approximation (VE) and vibronic spectrum. **b** | Absorption spectrum in the range 250–700 nm obtained as sum of vibronic spectra of the first eight lowest single electronic transitions. All theoretical spectra are red-shifted by  $450 \text{ cm}^{-1}$  (about 20 nm). Theoretical stick spectra have been convoluted by Gaussian functions with a half-width at half-maximum (HWHM) of  $500 \text{ cm}^{-1}$  (VE) or Lorentzian functions with a HWHM of  $250 \text{ cm}^{-1}$  (vibronic). Computed spectra adapted with permission from REF.<sup>160</sup>, Wiley.

The first term in Eq. 16,  $\bar{V}(\tau)$ , provides the ensemble average of the potential energy, and the second term adjusts the value of  $V_{\text{ref}}$  to ensure a nearly constant ensemble size  $N_w$  throughout the simulation. Finally,  $\alpha$  is an adjustable parameter. Once the ensemble has equilibrated, the time-averaged value of  $V_{\text{ref}}$  provides the zero-point energy of the system of interest.

It is important to recognize that  $V_{\text{ref}}$  fluctuates during the simulation, as FIG. 6a–c illustrates for  $H^+(\text{H}_2\text{O})_2$  (REF.<sup>163</sup>). The plots in FIG. 6a–c show the evolution of  $V_{\text{ref}}$  for three different combinations of time increments  $\Delta\tau$  and ensemble sizes  $N_w$ , where all simulations are propagated over the same total time. Generally, the size of the fluctuations of  $V_{\text{ref}}$  decreases as  $N_w$  or  $\Delta\tau$  increases, improving the quality of the results but also increasing computational time. Additionally, changing the value of  $\alpha$  tunes the size of the  $V_{\text{ref}}$  fluctuations, which we explore in FIG. 6c and Supplementary Figure 2. All dark blue plots in FIG. 6a–c have  $\alpha = 0.5 / \Delta\tau$ . FIGURE 6c shows that when  $\alpha = 0.5$ , the  $V_{\text{ref}}$  fluctuations are largest; as  $\alpha$  decreases to 0.1 or smaller, the size of the fluctuations remains roughly the same on the scale as the FIG. 6c plot. In the lower panel of Supplementary Figure 2 that focuses on a smaller range of propagation times, we find that decreasing  $\alpha$  removes the highest frequency fluctuations whereas a low-frequency oscillation of  $V_{\text{ref}}$  remains. The goal when selecting  $\alpha$  is to identify a value at which the high-frequency oscillations of  $V_{\text{ref}}$  roughly occur between three and ten time steps. This choice lessens the correlation of  $V_{\text{ref}}$  between subsequent time steps without increasing the magnitude of the  $V_{\text{ref}}$  fluctuations, and  $\alpha = 0.5 / \Delta\tau$  generally yields good results in this regard<sup>84,164,165</sup>.

The numbers shown in FIG. 6b provide the zero-point energy that is obtained by averaging  $V_{\text{ref}}$  over different ranges of  $\tau$ , with the numbers in parentheses representing the standard deviation among five independent simulations performed using these parameters. FIGURE 6b shows that the evaluated energy is relatively insensitive to how long the averaging is over, but the standard deviations are about half as large when  $V_{\text{ref}}$  is averaged over more than 10,000 atomic units in imaginary time. FIGURE 6d compares the evaluated zero-point energies for nine different combinations of ensemble sizes and time increments. We note that the smallest  $N_w$  value has the greatest uncertainty in its zero-point energy, and when both the smallest  $N_w$  and the largest  $\Delta\tau$  values are used, the simulation yields a zero-point energy that is inconsistent with the benchmark calculation (dotted line). The larger ensembles provide zero-point energies that agree with the benchmark results for all three time increments. However, as with the fluctuations of  $V_{\text{ref}}$ , the statistical uncertainties in the reported zero-point energies decrease for smaller  $\Delta\tau$  values and for larger ensembles, so a compromise must be made between accuracy and computational time.

In addition to the zero-point energies, DMC provides a powerful tool to obtain projections of the ground-state probability amplitude onto a desired coordinate. This is achieved by propagating the ensemble of walkers over a short period of imaginary time,  $\tau_{\text{DW}}$ , and identifying the fraction of the ensemble at  $\tau + \tau_{\text{DW}}$  that is traced to a particular walker in the ensemble at  $\tau$ . This number

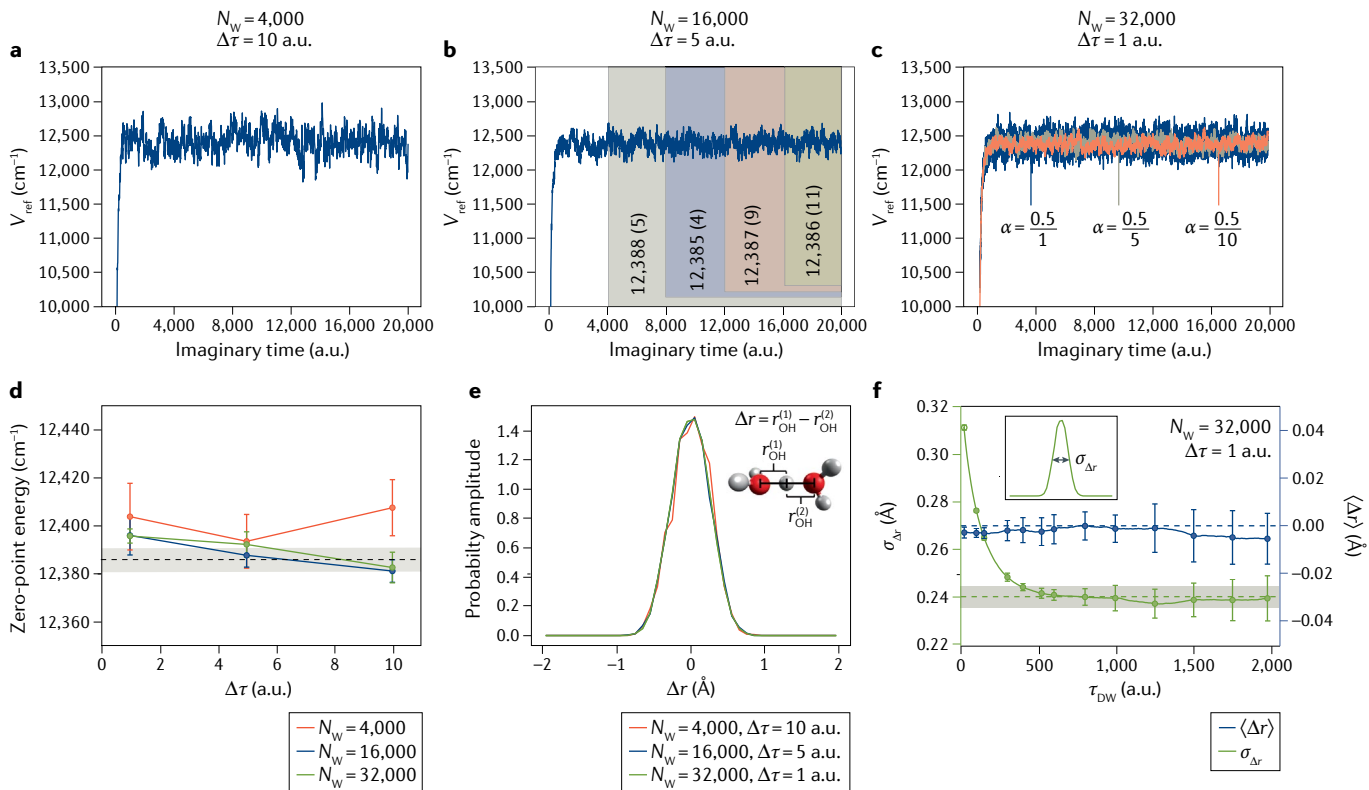


**Fig. 6 | Convergence properties of diffusion Monte Carlo.** **a–c**  $|V_{\text{ref}}$  values plotted as a function of imaginary time obtained from diffusion Monte Carlo (DMC) simulations with  $N_w = 4,000$  and  $\Delta\tau = 10$  a.u. (part a),  $N_w = 16,000$  and  $\Delta\tau = 5$  a.u. (part b) and  $N_w = 32,000$  and  $\Delta\tau = 1$  a.u. (part c). Part b also shows how the evaluated zero-point energy depends on how long  $V_{\text{ref}}$  is averaged (these values are also tabulated in Supplementary Tables 1–3). Part c shows how the size of the  $\alpha$  parameter affects the magnitude of the fluctuations in  $V_{\text{ref}}$ . **d** Calculated zero-point energy as a function of the time increment for ensemble sizes ranging from 4,000 (red) to 32,000 (green) walkers, and compared with the results obtained using  $N_w = 20,000$  and a time increment

of 10 a.u. (black dashed line, where grey shading indicates a  $5 \text{ cm}^{-1}$  uncertainty in that value). **e** Projections of  $\Psi^2$  onto  $\Delta r$  (see inset) as a function of ensemble size based on a calculation where the number of descendants is evaluated after  $\tau_{\text{DW}} = 520$  a.u. **f** Expectation value (blue) and standard deviation of  $\Delta r$ , plotted as a function of  $\tau_{\text{DW}}$ . Dotted blue and green lines provide reference values of 0  $\text{\AA}$  for the average and 0.240  $\text{\AA}$  for the standard deviation. Whereas the average value of  $\Delta r$  can be determined by symmetry, the standard deviation is obtained using an adiabatic DMC calculation<sup>83,166</sup>. All error bars and uncertainties reflect the standard deviations among five independent DMC simulations.

is proportional to the value of the wave function at the coordinates of the walker at  $\tau$ <sup>84,87</sup>, allowing us to use Monte Carlo integration to generate the desired projection of the probability amplitude  $\Psi^2$ . This approach is used to obtain the projection of the ground-state probability amplitude onto  $\Delta r$  (FIG. 6e inset), and the resulting distributions are shown in FIG. 6e for several values of  $N_w$  and  $\Delta\tau$ . As it is hard to differentiate among these results, the mean values of  $\Delta r$ , along with the standard deviation, are shown as functions of  $\tau_{\text{DW}}$  in FIG. 6f. The convergence of the results can be estimated by the plots in FIG. 6f that compare the computed values against independently obtained values of these quantities based on symmetry ( $\langle \Delta r \rangle$ , blue dotted line) or an alternative way to obtain expectation values ( $\sigma_{\Delta r}$ , green dotted line)<sup>83,166</sup>.

Extensions to DMC that enable the study of excited state energies and wave functions have also been developed<sup>16,167–169</sup>, although a discussion of these is beyond the scope of the present Primer.

#### Absolute configuration determination

Chiral spectroscopic techniques such as ORD, ECD, VCD and ROA play a fundamental role in determination of the absolute configuration. As spectra for enantiomers

are mirror images, the absolute configuration can be determined by comparing the calculated spectra with the experimental ones. In the simplest case, the spectra of the two enantiomers are calculated and compared with the experimental spectrum of one of the enantiomers, (+) or (−). The calculated spectrum in best agreement with the experimental spectrum defines the absolute configuration of the experimental enantiomer. As an example, the experimental and calculated VCD spectra for (+)-camphor and (1*R*,4*R*)-camphor are shown in FIG. 7a. Given the quantitative agreement between the calculated and experimental spectra, the absolute configuration of (+)-camphor is assigned to be 1*R*,4*R*. As these are enantiomers, it follows that (−)-camphor is (1*S*,4*S*).

Each of these chiral spectroscopies can be applied individually or in combination<sup>170–175</sup>. The advantage of using multiple methods is to provide complementary information, which is useful to distinguish diastereomers with multiple chiral centres, as one method may not be able to distinguish particular stereocentres. ORD, ECD and VCD were individually unable to unambiguously assign the absolute configuration of Hibiscus and Garcinia acids that each contain two chiral centres, whereas a combination of VCD with either ECD or

ORD was able to correctly assign the absolute configuration of both molecules<sup>170</sup>. Similarly, VCD and ROA (but not ECD) were able to correctly assign the absolute configuration of synoxazolidinone<sup>175</sup>, a marine antibiotic compound containing two chiral centres and one asymmetrically substituted double bond, resulting in a total of eight possible stereoisomers. FIGURE 7b–e shows a recent study on artemisinin<sup>173</sup>, an antimalarial drug containing seven chiral centres, which found that even though ROA and VCD could independently assign the correct stereochemistry, the combination of these two methods resulted in an even stronger unambiguous absolute configuration assignment (see VCD and ROA spectra in FIG. 7b,d).

For molecules containing multiple chiral centres and whose diastereomers predict similar spectra, the harmonic approximation, which is routinely used for VCD and ROA, may not be sufficient for a reliable absolute configuration assignment. This is the case for diplopyrone (FIG. 7f,g), a phytotoxic monosubstituted tetrahydropyranpyran-2-one containing four chiral centres, two of which were previously unassigned<sup>172</sup>. This molecule also possesses several low-energy conformers, further complicating the analysis of the spectra. In this case, ECD was not able to distinguish between the four possible diastereomers and the diastereomers predicted very similar harmonic VCD spectra. However, VCD spectra computed at the anharmonic level (FIG. 7f)

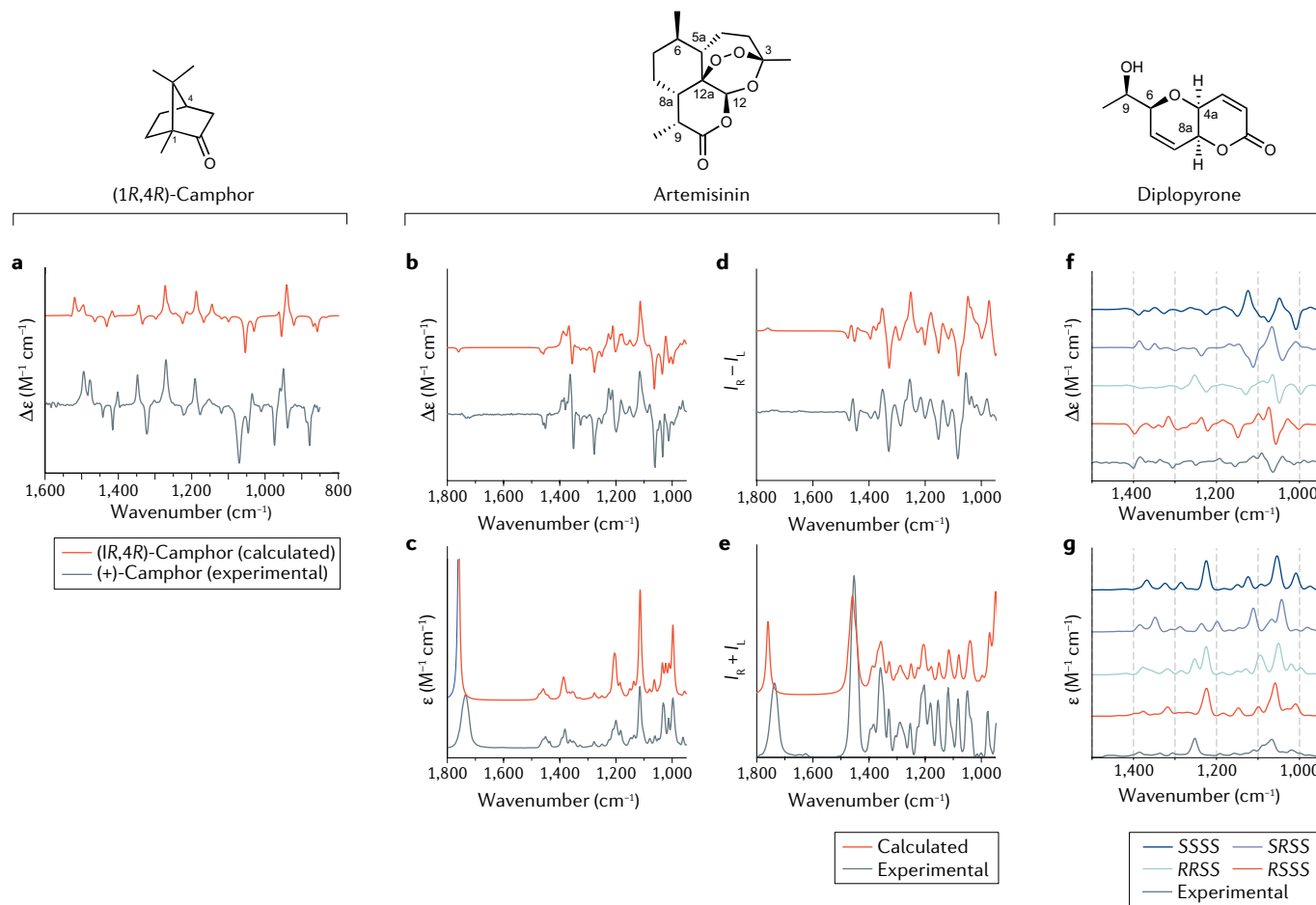


**Fig. 7 | Computed and experimental VCD and ROA spectra for the determination of absolute configuration.** **a** | Comparison of calculated and experimental vibrational circular dichroism (VCD) spectra for (1R,4R)-camphor and (+)-camphor, respectively. Calculated spectra are plotted using the Lorentzian line-shape function using a half-width at half-maximum (HWHM) of  $4\text{ cm}^{-1}$ . Experimental data, originally from REF.<sup>66</sup> and kindly provided by Frank Devlin (USC). **b–e** | Comparison of calculated and experimental VCD (part b), infrared (part c), Raman optical activity (ROA) (part d) and Raman (part e) spectra for (3R,5aS,6R,8aS,9R,12S,12aR)-artemisinin and (+)-artemisinin, respectively. Calculated spectra are plotted using the Lorentzian line-shape function using a HWHM of  $5\text{ cm}^{-1}$  for VCD/infrared and  $8\text{ cm}^{-1}$  for ROA/Raman. A molecule containing seven chiral centres should, in principle, have  $2^7 = 128$  diastereomers, but two of the chiral centres being fixed via an endoperoxide bridge reduces the diastereomers to  $2^6 = 64$ . Because half of these diastereomers are enantiomers, conformational analysis and spectra calculations were

performed for a total of 32 diastereomers. **f,g** | Comparison of calculated anharmonic and experimental VCD (part f) and infrared (part g) spectra of four diastereomers of diplopyrone and (+)-diplopyrone, respectively. The order of the chiral centres for each diastereomer label is 9, 6, 4a, 8a. As the agreement with respect to the experiment is best for the RSSS diastereomer, the absolute configuration is assigned to be (+)-(9R,6S,4aS,8aS)-diplopyrone. Calculated spectra are plotted using the Lorentzian line-shape function, using a HWHM of  $8\text{ cm}^{-1}$ . Part a adapted with permission from REF.<sup>66</sup>, under copyright © 2012 from VCD Spectroscopy for Organic Chemists by P.J. Stephens, F.J. Devlin and J.R. Cheeseman. Reproduced by permission of Taylor and Francis Group, LLC, a division of Informa plc. Parts b–e adapted with permission from REF.<sup>173</sup>, Royal Society of Chemistry. Parts f and g adapted with permission from REF.<sup>172</sup>, Fusè, M. et al. Unbiased determination of absolute configurations by vis-à-vis comparison of experimental and simulated spectra: the challenging case of diplopyrone. *J. Phys. Chem. B* **123**, 9230–9237 (2019). Copyright 2019 American Chemical Society.

were sufficiently close to the experiment to allow for a confident assignment of the two unknown chiral centres.

The comparison of calculated and experimental spectra is an important part of the assignment of the absolute configuration. Although this comparison can be performed visually, different approaches exist to remove bias and to quantify the degree of similarity. All of these methods rely on the calculation of a spectral overlap between the experimental and predicted spectra<sup>171,173</sup>. Another approach involves the analysis of the dissymmetry factor, defined as the ratio of  $\Delta\varepsilon$  and  $\varepsilon^{69,174,176}$ . Another measure of the reliability of the calculated vibrational spectra is the concept of robust modes, first developed for VCD<sup>177</sup> and later extended to ROA<sup>178</sup>. In this approach, a mode is determined to be robust if the rotational strength or scattering activity will not change sign due to small perturbations in either experiment or calculation.

Although the primary utility of chiroptical vibrational methods is to produce the spectra shown in FIG. 7, additional information can be extracted to help in the analysis and interpretation of the results. These include examining the vibrational transition current density associated with a molecular vibration<sup>179,180</sup> for VCD and computing atomic contribution patterns and group coupling matrices<sup>181</sup> for ROA.

### Applications

Although the list of possible computational spectroscopy applications is too long to even begin to enumerate, in this section we select some significant examples showing the potential of computational molecular spectroscopy from the spectroscopies addressed in this Primer.

### Astrochemistry

The role of spectroscopic techniques in the study of the interstellar medium (ISM) has grown rapidly in the past few decades, with rotational spectroscopy playing a critical role. Most of the understanding of the ISM — the gas and dust existing in the space between the stars of a galaxy — comes from Earth-based spectroscopic observations. Atoms and molecules in the gas phase constitute 99% of the ISM's mass, whereas the remaining mass is composed of silicate and carbonate grains<sup>182</sup>. At the low temperatures of the ISM, gas-phase particles emit radiation whose frequency spans from the gigahertz to the terahertz domains. Physically, the emitted quanta correspond to the transitions between rotational energy levels of the molecules. Each molecule can therefore be identified through its specific 'fingerprints', i.e. its rotational transitions<sup>182</sup>. With these molecules being ubiquitous in the ISM, the chemical composition, physical properties and the evolutionary stage of interstellar objects can be derived from radio-astronomical observations<sup>183</sup>. The laboratory data needed to guide astronomical observations and to discover new interstellar species are provided by rotational-spectroscopy laboratory studies<sup>184</sup> that are increasingly supported and complemented by quantum chemistry computations<sup>140</sup>.

The search for interstellar complex organic molecules (defined as species containing at least six atoms and composed of carbon, hydrogen, oxygen and/or

nitrogen<sup>185</sup>) can be assisted by the minimum energy principle stating that "the most stable isomer of a given chemical formula is always the most abundant in the ISM"<sup>186</sup>. A computational study of the relative stability of different isomeric (structural or conformational) species allows the screening of potentially observable molecules. In the case of conformers, the energy difference among the various conformers can be as small as a few kilojoules per mole. The size of the electric dipole moment therefore becomes an important parameter worth computing, as the intensity of rotational transitions scales with the square of the dipole moment component that allows the transition. The combination of the minimum energy principle and the magnitude of the electric dipole moment enables the straightforward identification of the most likely detectable interstellar complex organic molecules.

Once the species of interest is recognized, computational spectroscopy guides the experimental study by providing accurate predictions of the rotational parameters to be used for spectral simulations<sup>141,187</sup>. Although such calculations are highly accurate<sup>140</sup>, their accuracy is generally insufficient for them to directly guide astronomical searches and/or assignments. However, in some cases, quantum chemistry predictions can assess the detection of new astrochemical species, as is the case with the cyanobutadiynyl anion, C<sub>5</sub>N<sup>-</sup> (REF. 188). Owing to the difficulty of producing this species, no laboratory study of its rotational spectrum has been reported to date. C<sub>5</sub>N<sup>-</sup> has nonetheless been discovered in the envelope of a carbon-rich star thanks to the pinpoint match between astronomical observations and predictions based on high-level coupled-cluster calculations<sup>189</sup>.

The analysis of astronomical spectra can provide new information, but for this purpose the help of quantum chemistry calculations is often needed. As an example, investigating the hyperfine structure of the rotational spectrum is fundamental to gaining information on column densities, which provide a measure of molecular abundances. In rotational spectra, the hyperfine structure is due to interactions between the molecular electric and/or magnetic fields and the nuclear moments. The most important of these interactions is nuclear quadrupole coupling together with nuclear spin–rotation interaction. In addition, dipolar spin–spin interactions among different nuclear spins may also arise. In the case of molecular ions, experimental resolution is usually limited by the impossibility of reducing the working pressure inside the cell because of the ion-production process<sup>190</sup>, thus leading to the partial or even non-resolution of hyperfine structures, as shown in FIG. 8. Interstellar lines are instead very narrow. Therefore, when required, quantum chemistry calculations can be used to accurately predict the hyperfine structure of astronomical spectra, with the quantitative accuracy obtainable with state-of-the-art quantum chemistry calculations demonstrated in FIG. 8. Another significant example is CF<sup>+</sup>, where computed hyperfine parameters were used to assign the hyperfine structure of the astronomical rotational spectrum<sup>191</sup>.

Finally, appropriately modelling the ISM requires computing collisional rate coefficients for interstellar

---

### Nuclear quadrupole coupling

Interaction between the quadrupole moment of a nucleus and the electric-field gradient at this nucleus. Nuclei have a quadrupole moment when the nuclear spin is greater than 1/2. This interaction produces a hyperfine structure in the rotational spectra.

### Spin–rotation interaction

The interaction between the weak magnetic field generated by the end-over-end rotation of a molecule with the nuclear magnetic moment. The nuclear magnetic moment is present when the nuclear spin is non-null. This interaction produces a hyperfine structure in the rotational spectra.

molecules by the most abundant species (here, hydrogen and helium; also called colliders). Interstellar species are often far from a local thermodynamic equilibrium condition. The collisions occurring between molecular hydrogen or atomic helium and the molecule under consideration therefore significantly affect the population of rotational levels in the molecule and have an impact on the rotational transitions observed with radioastronomy<sup>192</sup>. In turn, the derivation of collisional data requires the computation of the PES of the molecule-collider with high accuracy.

### Weakly bound clusters and biomolecules

A wide and expanding computational spectroscopy application is the calculation of spectra for weakly bound clusters and biomolecules. This includes magnetic and electronic spectroscopy<sup>193,194</sup> in the broadest sense, but here we confine comments to vibrational spectroscopy with applications mainly in the near and far infrared region of the spectrum.

Advances in high-resolution infrared spectroscopy of small van der Waals molecules have stimulated very good agreement between theory and experiment<sup>195</sup>. This work started with rare gas atoms attached to diatomic molecules<sup>196</sup> but has extended to larger weakly bound clusters involving polyatomic molecules<sup>197</sup>. Clusters involving water molecules have received particular attention due to the importance of water throughout the sciences<sup>198</sup>. The water dimer is a key system and highly accurate fully dimensional PESs have been produced from sophisticated ab initio procedures<sup>199</sup>. These potentials have been used in converged calculations of vibrational states using appropriate basis functions for the different degrees of freedom and full-dimensional Hamiltonians with variational procedures. This has led to excellent agreement between theory and experiment for the spectra in the far infrared region of the water dimer<sup>200</sup>.

As the PES for the water dimer is the main component of potentials for larger water clusters, modelling these water clusters only requires additional and fairly simple three and four-body interactions between the different water molecules<sup>201</sup>. More challenging is the accurate calculation of the ro-vibrational states of water clusters larger than the dimer. Whereas conventional basis-set methods with variational procedures quickly become unwieldy, alternative procedures can quite accurately calculate some parameters of experimental interest, such as the rotational constants of the lowest vibrational states of clusters of different geometries and tunnelling splittings of vibrational states arising from identical minima on the PESs. DMC<sup>202–204</sup>, instanton<sup>205</sup> and path integral<sup>206</sup> procedures have been effectively applied on clusters up to  $(\text{H}_2\text{O})_8$  and have allowed detailed comparison with far infrared and microwave experiments.

The general importance of water in biology has meant that clusters of water with molecules of biological interest have been the subject of numerous calculations<sup>207</sup>. Methods such as DMC can be applied to calculate the structures of geometric isomers of biomolecules and their associated rotational constants<sup>208</sup>. Quantum chemistry calculations of infrared spectra for complexes such as

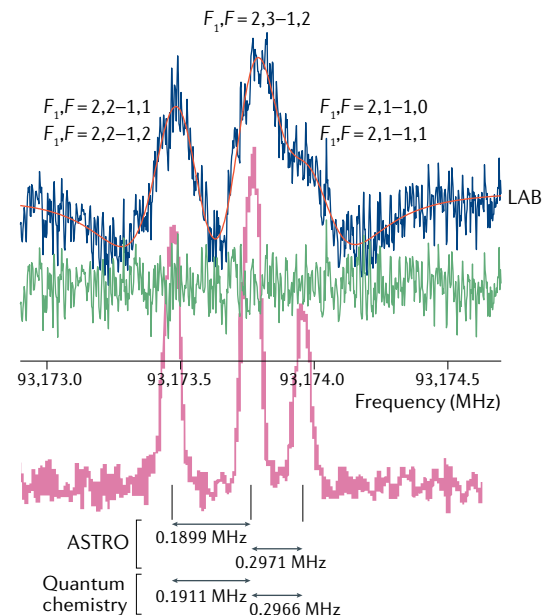


**Fig. 8 | Comparison of theory and experiment for the rotational spectrum of diazenylum cation.** A portion of the laboratory (LAB)<sup>190</sup> and astronomical (ASTRO, low-mass cloud core L1512 in Taurus<sup>261</sup>) spectrum of the first rotational transition ( $J=1-0$ , with  $J$  being the rotational quantum number) of the diazenylum cation ( $\text{N}_2\text{H}^+$ ) are compared. The actual comparison is between the red LAB spectrum (resulting from the line profile analysis of recorded spectrum in blue, with the green trace being the corresponding residual) and the ASTRO counterpart (pink line). The hyperfine splittings are reported and compared with the computed (quantum chemistry) values. Hyperfine structure is due to the presence of two nuclear quadrupolar nuclei, the nitrogen atoms. Quantum numbers  $F_1$  and  $F$  arise from the coupling schemes  $F_1 = J + I_{\text{N}_1}$  and  $F = F_1 + I_{\text{N}_2}$ , respectively, with  $I$  being the nuclear spin quantum number (=1 for nitrogen). Laboratory spectrum adapted with permission from REF.<sup>190</sup>, American Astronomical Society (IOP). Astronomical spectrum adapted with permission from REF.<sup>261</sup>, American Astronomical Society (IOP).

uracil–water have shown the importance of hydrogen bonding and anharmonic effects in these systems<sup>209</sup>.

For more complicated biomolecules, quantum chemistry, DFT and more approximate procedures such as quantum mechanics/molecular mechanics and semi-empirical force fields have been applied<sup>210</sup>. The simplest approaches only calculate the harmonic frequencies but anharmonic aspects have also been considered using various quantum mechanics procedures including VPT2 and the vibrational self-consistent field<sup>211</sup>. FIG. 9 shows an example of a recent calculation<sup>212</sup> of the near infrared spectra of the crystalline structures of DNA bases, where results from deperturbed VPT2 calculations were compared in detail with experiments. The calculations in FIG. 9 demonstrate the power of computations in predicting and interpreting the vibrational spectra of molecules of biological interest. Assignment of the different overtones and combination bands found in this high-energy region ( $4,000$ – $7,500 \text{ cm}^{-1}$ ) and their interpretation in terms of structural motifs would be

Molecular mechanics  
Classical model to predict the energy of a molecule as a function of its conformation.

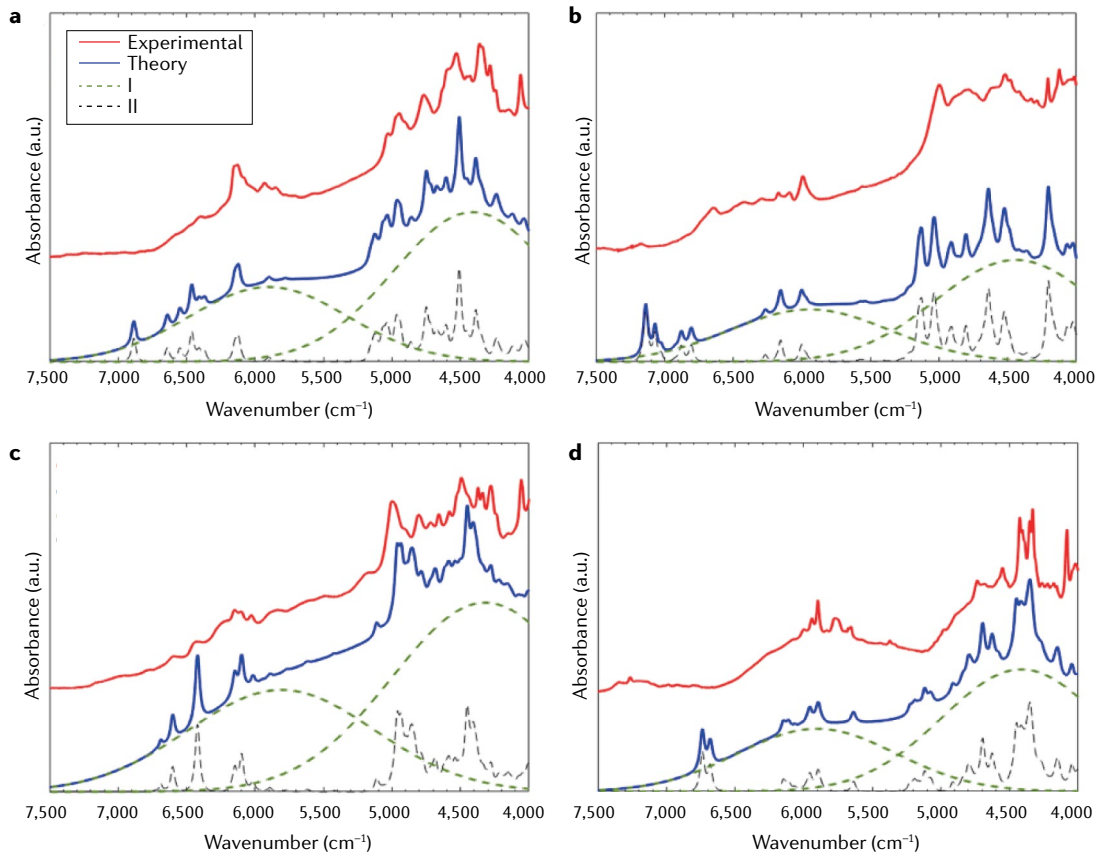


**Fig. 9 | Comparison of theoretical and experimental near infrared spectra of crystalline DNA bases.** a–d | Experimental and calculated near infrared spectra of crystalline adenine (part a), cytosine (part b), guanine (part c) and thymine (part d) in the 4,000–7,500 cm<sup>-1</sup> region<sup>212</sup>. Adapted from REF.<sup>212</sup>, CC BY 4.0 (<https://creativecommons.org/licenses/by/4.0/>).

#### Orbital splittings

Splittings of specific orbitals due to external factors (for example, electric or magnetic field).

#### Crystal field theory

The splitting of the (relativistic) many-particle multiplet states of an ion in a  $d^n$  or  $f^l$  configuration incurred by the electrostatic interaction with its coordinating ligands that are treated as point charges.

#### Multiplets

An ensemble of many particle states that arise from the distribution of a given number of electrons among sets of degenerate atomic or molecular orbitals under the action of the electron–electron (and perhaps the spin–orbit coupling) interaction.

#### Spin–orbit coupling

The coupling between the spin and the orbital angular momenta.

#### Slater determinant

Representation of a many particle ‘mean-field’ wave function in terms of the antisymmetrized products of single-electron wave functions (molecular orbitals).

very difficult (and questionable) without the help of quantum chemistry computations.

#### Spectroscopy of $d$ and $f$ elements

The spectroscopy of  $d$  and  $f$  elements introduces new experimental and theoretical challenges that are not easily met. At the heart of the challenges associated with these elements is the fact that they can exist in various oxidation states that lead to spectroscopically well-defined  $d^n$  and  $f^l$  configurations ( $n$  = number of electrons in the  $d$  or  $f$  shell).

Given the high effective nuclear charge experienced by  $d$  or  $f$  electrons, the corresponding orbitals are compact. Compared with the strong bonds formed between main group elements, the  $d$  and  $f$  elements therefore bind comparatively weakly through their orbitals to the surrounding ligands. Thus, the ligand environment induces limited orbital splittings. This has been exploited very fruitfully in the phenomenological model of crystal field theory<sup>213</sup>. In crystal field theory, the  $d$  or  $f$  electrons are treated as free ions perturbed by an electrostatic field created by the surrounding ligands. Although quantitatively unrealistic, the theory captures the essentials of  $d$  ( $f$ )-element electronic structure. Thus, the combination of a partially filled  $d$  or  $f$  shell and limited ligand field splittings leads to a series of low-lying electronic states formed by distributing  $n$  electrons between the available orbitals while simultaneously coupling electron

spins in all possible ways to result in a net total spin. On top of the complexity arising from a large variety of multiplets,  $d$  and  $f$  elements are heavy. The effects of relativity become much more prominent in these compounds, and whenever there are unpaired electrons, a treatment of the spin–orbit coupling becomes mandatory for theoretical spectroscopy<sup>13</sup>. The electronic complexity is necessarily also reflected in the observed spectra. Throughout the range of available techniques ranging from hard X-rays (10<sup>4</sup> eV) down to microwaves and radiowaves (10<sup>-11</sup>–10<sup>-9</sup> eV), the spectra typically show a high amount of spectral crowding due to the multitude of final states that can be reached in the respective spectroscopic transitions. In addition, the spectra are difficult to interpret because of the complexity of the electronic states involved, and therefore require a high amount of expertise to be interpreted correctly.

The complex electronic multiplets in the presence of relativistic effects are not easily reproduced even in a semi-quantitative way by the available quantum chemistry methods<sup>214–216</sup>. In those cases where there are (near-)orbital degeneracies (as readily predicted by crystal field theory), there may not be a single Slater determinant that is an appropriate starting point for the description of the electronic ground state. In such a case, all single-reference determinant based methods (including DFT) fail to describe the electronic structure of either the ground or the excited states correctly. Typically, not

**Circular dichroism**

Dichroism (splitting of a beam of light into two beams with different wavelengths) involving circularly polarized light, that is, the differential absorption of left and right-handed light.

**Magnetic circular dichroism**

Circular dichroism induced by a static, longitudinal external magnetic field.

**SQUID**

A magnetometer based on superconducting loops used to measure very low magnetic fields.

**Electron paramagnetic resonance**

A synonym of electron spin resonance.

even the number of reachable final states tends to be correct<sup>13,15</sup>. Thus, DFT has many serious shortcomings in the field of *d* and *f*-element theoretical spectroscopy. These shortcomings were highlighted in some reviews over a decade ago and stand essentially unchanged today<sup>13,17,21</sup>.

The occurrence of a rich multiplet structure together with the prominence of relativistic effects opens up rich opportunities for experimental spectroscopy (see FIG. 10). Magnetic low-energy spectroscopies, such as NMR and ESR, can probe the magnetic sublevels of the electronic ground-state multiplets, whereas modern magnetometry is extensively used to study the magnetic properties of *d* and *f* elements for molecular magnetism. Electronic spectroscopies including UV–Vis, circular dichroism and magnetic circular dichroism or resonance Raman provide in-depth insights into the electronic structure of these species. Finally, as there are typically only a few atoms of a given element present in the compound, element-specific techniques such as Mössbauer or X-ray absorption/emission spectroscopies are very widely used<sup>17</sup>. All of these methods provide detailed fingerprints of the geometric and electronic structure of the systems under investigation. More importantly, each one of these techniques is sensitive

to different geometric and electronic structure details, leading to a host of experimentally available electronic structure information. However, in order to develop the full information content of these spectra, spectral interpretations require quantum chemistry. A successful study results in insight into the experimentally calibrated electronic structure of the investigated species, be they stable entities or reaction intermediates. As discussed elsewhere, this leads to insights that cannot be obtained from the pure calculation of total energies<sup>218,219</sup>.

**Case study of magnetic Co(II) tetrathiolates.** Coordination complexes of Co(II) ions (*d*<sup>7</sup> configuration) are well known in coordination chemistry and have been routinely characterized with magnetic measurements such as SQUID, electron paramagnetic resonance (EPR) or magnetic circular dichroism spectroscopy. In an approximately tetrahedral environment, the ground state has a total spin of  $S = 3/2$ . A cursory look at the ion  $[\text{Co}(\text{S}-\text{Ph})_4]^{2-}$  also does not reveal anything out of the ordinary. However, this ion shows slow magnetic relaxation at zero magnetic field, the signature behaviour of the thought-after single-molecule magnet behaviour<sup>220</sup>.  $[\text{Co}(\text{S}-\text{Ph})_4]^{2-}$  is the first mononuclear compound to show this behaviour whereas for several decades it was believed that only large, oligonuclear transition metal clusters could show single-molecule magnet properties (see REF.<sup>221</sup>).

Studies of the magnetic properties of two different salts containing  $[\text{Co}(\text{S}-\text{Ph})_4]^{2-}$  coupled to quantum chemical calculations were subsequently reported<sup>222,223</sup>, and are illustrated in FIG. 11. Surprisingly, only  $[\text{Co}(\text{S}-\text{Ph})_4](\text{P}(\text{Ph})_4)_2$  showed single-molecule magnet behaviour, whereas  $[\text{Co}(\text{S}-\text{Ph})_4](\text{N}(\text{Et})_4)_2$  did not. The experimental investigation attributed this to the Co(II) ion P(Ph)<sub>4</sub> having large and negative zero-field splitting, whereas the N(Et)<sub>4</sub> salt had small and positive zero-field splitting. The magnetic properties of both structures were reproduced with excellent accuracy through complete active space self-consistent field (CASSCF)/NEVPT2 calculation with inclusion of spin-orbit coupling. Furthermore, the ab initio ligand field theory method allowed for the ligand field parameters to be deduced from the large-scale wave function-based ab initio calculations. The calculations revealed that the origin of the radically different behaviour is a subtle distortion that causes the environment of the Co(II) ion in the P(Ph)<sub>4</sub> salt to be elongated and tetrahedral, whereas in the N(Et)<sub>4</sub> salt the Co(II) ion is in a compressed tetrahedral structure. The changes in the *d*-orbital splitting pattern are then sufficient to cause the dramatic switch of magnetic properties, as predicted by ligand field theory. The origin of the dramatically different behaviour can thus be traced back to weak intermolecular interactions in the second coordination sphere of the cobalt. These initial insights spurred further investigations of Co(II) complexes (for example, REF.<sup>224</sup>). This study of cobalt salts summarized in FIG. 11 demonstrates that a large body of complex and initially puzzling experimental observations can be quantitatively interpreted in a unified manner through large-scale multi-reference ab initio calculations. Moreover, the results of these

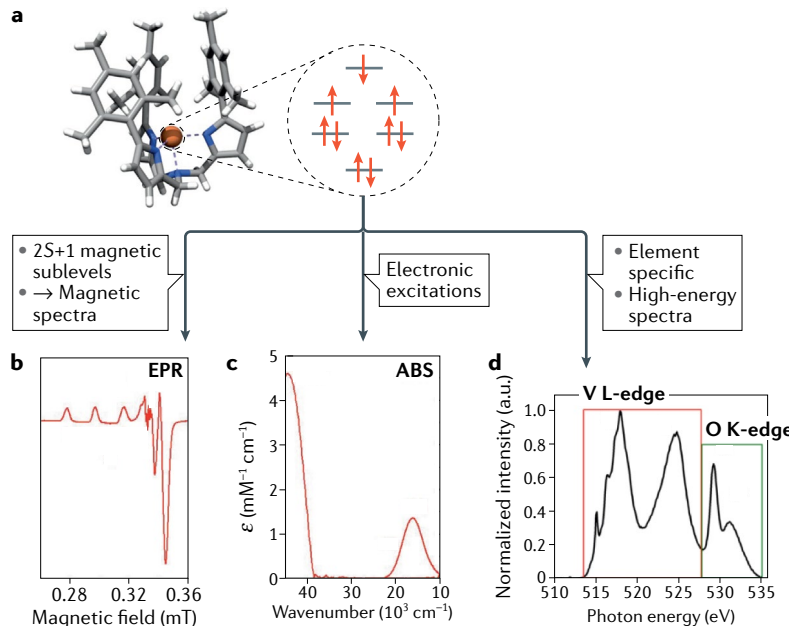


**Fig. 10 | Partially filled *d* and *f* shells lead to complex multiplet structures and rich spectroscopic phenomena.** **a** | Geometric structure (left panel: grey, carbon; white, hydrogen; blue, nitrogen; brown, transition metal) imposes a distinctive splitting of the molecular orbitals that are based on the transition metal *d* orbitals (right panel). **b–d** | Distribution of the *n* electrons in a *d*<sup>*n*</sup> configuration gives rise to a multitude of electronic states that can be probed with optical or magnetic spectroscopy. Among these, the most prominent are electron paramagnetic resonance (EPR) (part **b**), absorption (part **c**) and X-ray absorption (part **d**) spectra. EPR spectroscopy probes the net electron spin caused by the unpaired electrons of the electronic ground state. ABS (previously referred to as OPA) probes transitions of electrons between valence orbitals, including the metal *d*-based orbitals. X-ray spectroscopy probes excitations from deep core electrons on the transition metal centre(s) into the empty or half-filled valence orbitals. As the core levels vary systematically along the periodic table, this provides a highly sensitive element specific probe of the system under investigation. Parts **b** and **c** adapted with permission from REF.<sup>262</sup>, Wiley.

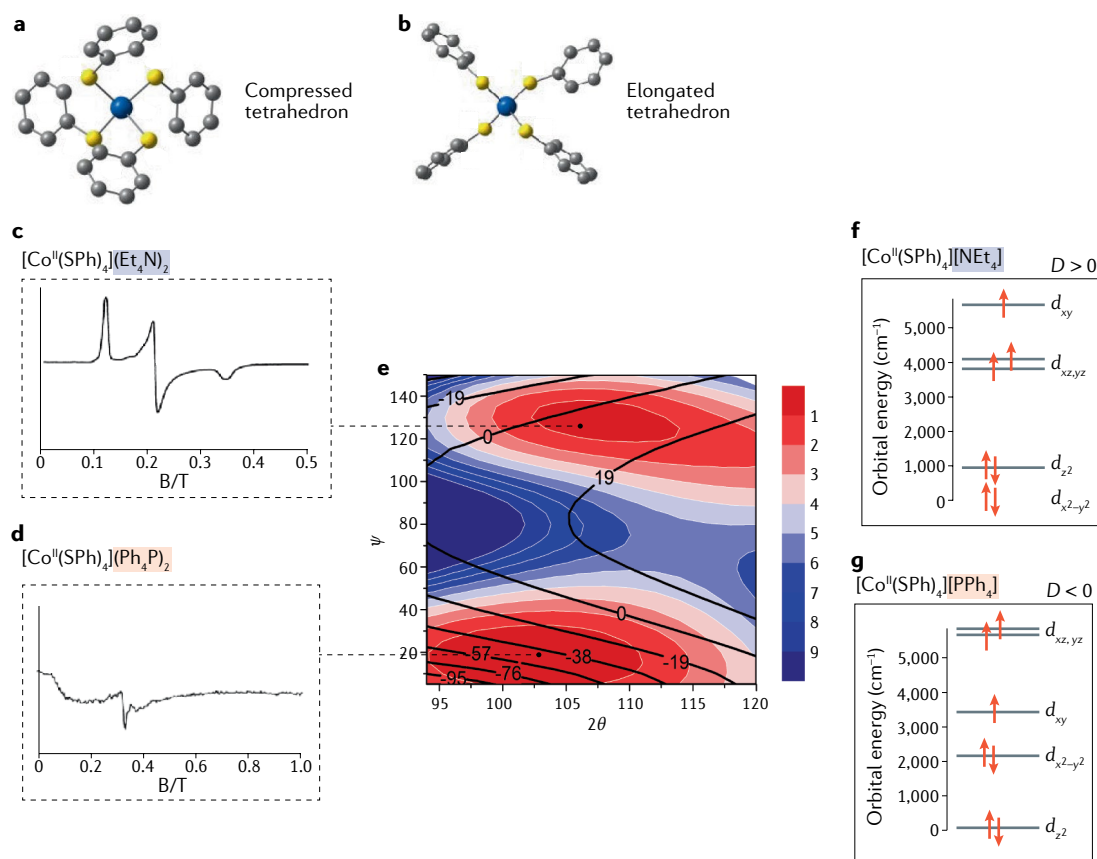


**Fig. 11 | Computational chemistry in conjunction with ab initio ligand field theory can be used to understand subtle and complex spectroscopic phenomena.** **a,b** Two structures of  $[\text{Co}(\text{S-Ph})_4]^{\text{2-}}$  found in the  $(\text{Et}_4\text{N})_2$  and  $(\text{Ph}_4\text{P})_2$  salts reflecting compressed and elongated tetrahedra respectively. **c,d** Radically different electron paramagnetic resonance spectra of the two species demonstrating their different electronic structures. **e,f** Effective  $d$ -orbital splitting patterns deduced from complete active space self-consistent field (CASSCF)/NEVPT2 ( $N$ -electron valence state perturbation theory to the second order) calculations for the two structures effectively explaining the origin of the very different  $D$  values. **g** Potential energy and property surface (zero-field splitting (ZFS) value) for two key angles describing the distortion into flattened and elongated tetrahedra in  $[\text{Co}(\text{S-Ph})_4]^{\text{2-}}$ . There are two shallow minima associated with qualitatively different  $D$  values as reflected in their electron spin resonance (ESR) spectra (parts **a** and **b**) and readily understood from quantum chemical calculations (parts **c** and **d**). Part **e** adapted with permission from REF.<sup>223</sup>, Suturina, E. A., Maganas, D., Bill, E., Atanasov, M. & Neese, F. Magneto-structural correlations in a series of pseudotetrahedral  $[\text{Co}^{\text{II}}(\text{XR})_4]^{\text{2-}}$  single molecule magnets: an ab initio ligand field study. *Inorg. Chem.* **54**, 9948–9961 (2015). Copyright 2015 American Chemical Society.

#### Zero-field splitting

The lifting of the degeneracy of the  $2S+1$  magnetic sublevels of a spin multiplet with total spin  $S$  in the absence of a magnetic field, caused by the effects of spin-orbit coupling and electron-electron spin-spin interactions.

**Ab initio ligand field theory**  
A method connecting the results of ab initio calculations with the parameters entering ligand field theory.

#### Ligand field theory

A semi-empirical ‘perturbed ion’ model, based on crystal field theory, that describes the electronic structure and properties of transition metal complexes.

calculations can be translated concisely into a familiar chemical language through the ab initio ligand field theory procedure.

#### Reproducibility and data deposition

Here, we discuss different levels of issues with data reproducibility and deposition.

The first level is the definition of a general standard for the inputs and outputs of electronic structure codes; this was discussed, for instance, in the MolSSI workshop. There are an increasing number of large-scale international and interdisciplinary collaborations, which often involve shared infrastructures and multi-user facilities and result in massive amounts of data. To enhance these collaborations, there is a strong need to integrate and standardize computational codes starting from a common syntax and/or language. An example in this direction is provided by the VMS project<sup>21</sup>, which aims to integrate several spectroscopic techniques and provide a user-friendly interface for different quantum chemistry

programs (see, for example, the module dedicated to rotational spectroscopy<sup>142</sup>).

The second level is the compilation and management of highly accurate results for small (two to four atoms) molecules, which can rival the corresponding experimental data<sup>34</sup>. Outside this narrow size range, theoretical models and computational procedures for computational spectroscopy are always based on approximations and assumptions, which need to be correctly recognized in the applications to realistic systems. However, small molecules can represent suitable fragments for benchmarking less refined methods and defining transferable correction factors for fragments of larger molecules<sup>225</sup>. Combining benchmark calculations and transferable correction factors paves the way towards the set-up of public databases of molecular structures and spectroscopic properties. One example is provided by the database of semi-experimental equilibrium structures.

The third level concerns the lines to be followed for the spectroscopic characterization of large systems,

**Template approach**

A model in which the structure of a molecular system is refined with reference to suitable fragments, whose structures are accurately known.

**Force constants**

Derivatives of the potential energy with respect to nuclear coordinates evaluated at the minimum structure, for example, the quadratic force constant is the second derivative.

which are of increasing interest to different scientific communities. The available results for an adequate number of medium-sized systems should be organized in sets of comparable accuracy by clustering techniques employing widely accepted general criteria. For some properties, such as energies, the general definition of platinum, gold and silver standards<sup>226</sup> is more or less accepted. These definitions are based on the accuracy provided. For example, CCSD(T) calculations extrapolated to the complete basis-set limit define the gold standard. The silver standard provides the best approximation to the gold standard at a reduced computational cost, whereas the platinum standard improves the gold standard by adding further corrections (such as higher-order coupled-cluster terms). However, such standards have not been developed for most spectroscopic properties. For instance, fully quantitative results for high-resolution spectroscopic techniques such as rotational spectroscopy are still out of reach even for semi-rigid triatomic and tetratomic systems<sup>227</sup>, because the required computations are unaffordable. However, new methods based on the template approach possibly coupled with machine learning tools appear quite promising<sup>225,228</sup>. As an example, in the field of vibrational spectroscopies, some methodologies (such as VPT2 treatments based on an anharmonic description of the PES at a suitable level of theory<sup>34</sup>) can reach an accuracy within 10 cm<sup>-1</sup> and are also applicable to large-sized systems with the help of linear scaling<sup>229,230</sup> and reduced dimensionality<sup>231</sup> techniques. Here, the compilation and management of databases (extending those mentioned for the second level to large molecules) is of current interest in the field. More work in this direction should be performed with compilations of spectroscopic parameters for molecules including heavy elements and for different spectroscopies. For spectroscopic transition intensities, the definition of widely accepted standards is still missing. Another important issue when dealing with large systems is their flexibility, which requires the implementation of effective approaches to search for energetically low-lying structures, for example conformers or isomers<sup>150</sup>. In fact, a key point towards data/spectra reproducibility is the understanding of which of these conformers or isomers contribute to the overall spectroscopic signal. However, we are still far from any general definition of classes of methods/models achieving a desired accuracy.

Focusing on the integration of levels two and three, an interesting option would be to simulate and store overall spectra instead of databases collecting lists of spectroscopic parameters. Another step forward would be the set-up of compilations combining results of different spectroscopies having comparable accuracies for use in assisting experimental work, which increasingly integrates the use of different techniques.

Another issue is the role of environmental effects, such as solvents. Environmental effects should be analysed for different properties and/or solvents to determine the most appropriate model for the specific case under consideration. Indeed, when the spectroscopic investigation is carried out in solution or, more generally, in a condensed phase, data reproducibility requires a full account of the environmental effects. For instance,

the polarizable continuum model<sup>34</sup> can be employed to describe innocent solvents at a negligible additional cost with respect to the corresponding simulation in vacuo. Such a model can be improved by incorporating a reduced number of explicit solvent molecules<sup>151</sup>, provided that they occupy well-defined positions and are quite strongly bonded to the solute. In this respect, topological models for the automatic definition of the number and position of strongly bonded solvent molecules are under active development<sup>232</sup> and the definition of widely accepted standards would be a very important achievement.

Finally, although the issue of a general standard addressed above (first level) is a basic need for collaborations, we want to make a note on the information accompanying publications. This does not need to involve program outputs, as the collection of spectroscopic parameters (normally in the form of tables) is usually exhaustive. Cartesian coordinates for the molecular systems investigated are generally provided, whereas the force constants describing a portion of the PES are more rarely reported.

**Limitations and optimizations**

Since its very beginning, computational spectroscopy has focused on deriving spectroscopic parameters to support the analysis of experimental spectra because interpretation of experimental data is often a difficult task. This is because the observed spectroscopic behaviour derives from the interplay of different effects, whose specific roles are difficult to disentangle. Furthermore, the theoretical model used for spectral interpretation may be oversimplified.

Approaches that push the resolution of the electronic and nuclear problems to the limit ensure rigorous analyses, quantitative results and correct interpretations of the spectroscopic outcomes. However, such approaches involve high computational costs and efforts, and are therefore restricted to small, isolated molecules. Increasing the system size and complexity often requires a sacrifice of accuracy for interpretability, thus leading to qualitative descriptions. In such cases, the main limitation is an oversimplification that might lead to the right answer for the wrong reason, which means obtaining the correct reproduction of the spectral features based on the wrong spectroscopic parameters. In turn, this might also mean derivation of the wrong physico-chemical properties, or even incorrect interpretation of what molecular species are actually observed. The only way to mitigate this is to try to apply a physically sound model and take corrective actions based on similar (but smaller) systems already investigated. However, the selection of the fragments and the treatment of the boundary among them are open questions that require considerable experience, good knowledge of the system to be investigated and, above all, further algorithmic developments and implementations.

Modern computational spectroscopy aims to bridge the gap between sophisticated experimental techniques and oversimplified analyses while also exploiting visualization and simulation techniques. An interesting example is provided by oxirane derivatives, whose spectral

features cannot be described by more simplified theoretical models. Today, state-of-the-art simulations of infrared, Raman, VCD, ROA, one-photon absorption and ECD spectra are in good agreement with their experimental counterparts and reconcile theory and experiment<sup>35,112,233,234</sup>.

Accurate methodologies have been developed for the treatment of small to medium-sized molecular systems (see, for example, REFS<sup>34,150,235</sup>), with linear-scaling and hybrid approaches allowing for their extension to larger systems. However, a current challenge for computational spectroscopy tools is represented by large flexible molecules, for which the analysis of the conformational PES is the first obstacle to be overcome. In order to correctly interpret the spectroscopic features of large flexible molecules, the knowledge of the structures contributing to them is mandatory. In this respect, the past decade has seen significant progress thanks to stochastic (molecular dynamics or Monte Carlo) techniques<sup>150</sup> and machine learning algorithms<sup>228,232</sup> that have helped derive an exhaustive account of the number and type of conformers relevant to spectroscopic analysis.

In spectral simulations, the number and types of LAMs still strongly limit accuracy. Although a decoupling (or a minimization of the coupling) between small amplitude motions and LAMs together with a variational treatment of the LAM modes can lead to accurate spectroscopic treatment, this approach is currently only effective for one LAM<sup>236</sup>. In addition, another issue is the level of theory for the description of the portion of PES (or PESs) required for the spectroscopic technique under consideration. For medium-sized molecular systems, the scaling of most of the accurate quantum chemistry models is prohibitive but composite schemes often provide an effective solution. For larger systems, a possible solution is offered by fragment-based approaches such as molecules in molecules<sup>236</sup>, which is a multilevel partitioning approach coupled with electronic structure studies at different levels of theory with the final aim of providing a hierarchical strategy for systematically improving the computed results. In parallel, further reliability improvements of methods rooted in DFT, such as double-hybrid functionals, long-range corrections and so on<sup>237</sup>, and the development of linear-scaling techniques, especially for exact exchange<sup>238</sup> and MP2 (REF.<sup>239</sup>), pave the way towards more reliable computations for large systems. Finally, explicitly correlated F12 treatments<sup>105</sup> reduce the basis-set dimensions in electronic structure computations and improve the reachable accuracy. A further step is provided by local correlation treatments based on pair natural orbitals<sup>106,107</sup>, which — as mentioned above — improve the scaling of coupled-cluster treatments with the number of electrons.

Although we cannot exhaustively address all of the limitations and optimizations for computational molecular spectroscopy in this section, we note that the accurate spectroscopic characterization of open-shell species is more challenging than that of their closed-shell counterparts, regardless of the size of the molecular system under consideration<sup>240</sup>. The situation is even more complex for systems showing large static correlation

effects such as, for example, the low-spin states of most transition metals. Methods rooted in the density matrix renormalization group<sup>136</sup> or quantum Monte Carlo<sup>241</sup> approaches are good alternatives with respect to multi-reference methods and open promising routes towards effective treatments.

## Outlook

Ongoing hardware and software developments allow the study of spectroscopic outcomes for several systems and processes of scientific and technological interest with an accuracy simply unthinkable even 10 years ago. The range of applications of computational spectroscopy has also considerably widened to now include fields such as astrochemistry<sup>242</sup>, atmospheric chemistry<sup>243</sup> or catalysis<sup>218</sup>. However, the historical dichotomy between accuracy and interpretability (not to speak of feasibility and user-friendliness)<sup>34</sup> remains one of the toughest obstacles against the definitive transformation of computational spectroscopy from a highly specialized field to a general-purpose tool aiding both theoretically and experimentally oriented scientists in their research work. Indeed, to solve this dichotomy, state-of-the-art spectroscopic investigations usually involve the contemporary use of several experimental techniques and the proposal and implementation of new and highly sophisticated computational tools. Today, what is needed is extending accurate evaluations of spectroscopic parameters from small semi-rigid closed-shell systems containing light atoms in the gas phase<sup>235</sup> to a general workflow for the spectroscopic characterization of large, flexible chromophores in condensed phases<sup>244</sup>. Although most of the building blocks for this procedure are already available, they have not yet been integrated into a robust, general and user-friendly tool.

One aspect to consider is the extension and validation of composite models for electronic structure calculations to transition metals and heavy atoms, large systems, open-shell species and excited electronic states. Possible routes to achieve this include explicitly correlated coupled-cluster approaches<sup>105,245</sup>, localized treatments of correlation (for example, using local pair natural orbitals)<sup>229,230</sup>, effective treatment of static correlation<sup>136,246</sup>, further improvements of density functionals for comprehensive scans of PESs<sup>247</sup> and reliable structure and force-field evaluations<sup>237</sup>, and more effective treatments of excited electronic states<sup>248,249</sup>.

Another important aspect to consider is the vis-à-vis comparisons between computed and experimental spectra, which is probably the best way to exploit the interplay of experiment and theory. These comparisons include positions and heights/intensities of band maxima, but also spectral shapes<sup>61</sup> and the extension of such comparisons to all possible spectroscopies. This, in turn, requires accurate yet effective evaluations of all parameters needed by different spectroscopic techniques<sup>133,250</sup> and their post-processing.

To improve the spectroscopic analysis of flexible molecules, in particular for rotational and vibrational spectroscopies, general-purpose treatments of their spectra in terms of curvilinear internal coordinates, possibly coupling the variational treatment of LAMs with

**QM/QM'**

A fundamental theory of contemporary physics that provides a description of the properties of the matter at the atomic and subatomic level. The slash is used to denote that two levels of treatments are employed and implies a partitioning of the system (QM', a different quantum mechanics level).

**Perturbed matrix method**

A perturbative model in which the environmental effects on a quantum centre are described in terms of the CIS (configuration interaction singles) method, whose elements are the energies of the isolated solute perturbed by the electric field produced by the different configurations of the solvent issuing from a molecular dynamics simulation.

the perturbative treatment of small amplitude motions, need to be developed and implemented<sup>247,251</sup>. A promising alternative is offered by integrated treatments of electronic and high-frequency nuclear motions by means of nuclear-electronic orbitals<sup>252</sup>. For absorption and emission electronic spectroscopies and their chiral counterparts, the extension of anharmonic vibronic models<sup>253</sup> is an important step forwards to be able to characterize biomolecules.

Looking forwards, we should aim for effective coupling between explicit dynamic treatment of soft degrees of freedom — such as torsions around single bonds, ring puckerrings and solvent fluctuations — involving large-mass moieties (for which classical equations of motion are fully adequate) and quantum-mechanical treatment of hard degrees of freedom<sup>254</sup>. These developments will allow the accurate yet effective treatment of large flexible systems in condensed phases, which is very difficult with current software and hardware.

Another important task is the integration of the variational evaluation of large-scale deformations using quantum mechanics (QM), QM/QM' or QM/MM (MM stands for molecular mechanics) for different conformers and/or different topologies of solute–solvent interactions in the cybotactic region with the perturbative evaluation of fluctuations within different basins<sup>151</sup> by using, for example, the perturbed matrix method. In this case, clever coupling of variational and perturbative approaches will strongly reduce the computer requirements in terms of both time and memory without sacrificing the accuracy of the overall computation.

For ro-vibrational spectroscopy, effectively determining partition functions and/or density and the number of states beyond the rigid-rotor/harmonic-oscillator model<sup>255,256</sup> will allow the computation of accurate

thermodynamic functions and reaction rates for flexible systems, possibly in condensed phases.

Implementing artificial intelligence tools for sampling PESs after training with reference and state-of-the-art quantum chemistry results paves the way towards accurate energies, structures and force fields for both local minima and transition states at a cost comparable with that of inexpensive molecular mechanics methods<sup>228</sup>. In addition, implementing immersive virtual and augmented-reality tools for general spectroscopic study set-ups and interactive analysis of the results<sup>257</sup> can revolutionize the field (as well as many others) by bringing the objects under study to the same spatio-temporal scale of human beings. In a more distant future, effective use of quantum computing will improve the rate of state-of-the-art techniques<sup>258</sup>. As an example, the exact solution of Schrödinger's equation has intrinsic exponential scaling and the most accurate quantum chemistry techniques scale as high powers (at least 10<sup>8</sup>) of the number of basis functions; although the speed of traditional computers scales linearly with the number of processors, the scaling of quantum computers is, in principle, exponential.

In summary, in this Primer we have focused on a selection of molecular spectroscopic techniques to present the foundations of computational spectroscopy as well as some significant results and applications. We have also addressed the fundamental role of computational spectroscopy in supporting and complementing experimental investigations. We have critically analysed current limitations and possible improvements to the technique and have concluded with an exhaustive presentation of future perspectives and needs.

Published online: 27 May 2021

- Nafie, L. A. in *Vibrational Optical Activity: Principles and Applications* (Wiley, 2011). **This book provides a comprehensive description of the underlying theory of the chiroptical spectroscopic methods VCD and ROA, and includes computational and experimental aspects as well as applications.**
- Merkt, F. & Quack, M. *Handbook of High-Resolution Spectroscopy* (Wiley, 2011).
- Laane, J. *Frontiers of Molecular Spectroscopy* (Elsevier, 2008).
- Berova, N., Nakanishi, K. & Woody, R. W. *Circular Dichroism: Principles and Applications* 2nd edn (Wiley-VCH, 2000).
- Rijss, A. M. & Oomens, J. *Gas-Phase IR Spectroscopy and Structure of Biological Molecules. Topics in Current Chemistry* Vol. 364 (Springer International, 2015).
- Pulay, P., Meyer, W. & Boggs, J. E. Cubic force constants and equilibrium geometry of methane from Hartree–Fock and correlated wavefunctions. *J. Chem. Phys.* **68**, 5077–5085 (1978).
- Obenchain, D. A. et al. Unveiling the sulfur–sulfur bridge: accurate structural and energetic characterization of a homochalcogen intermolecular bond. *Angew. Chem. Int. Ed.* **57**, 15822–15826 (2018).
- Caminati, W. in *Handbook of High-Resolution Spectroscopy* (eds Merkt, F. & Quack, M.) (Wiley, 2011).
- Park, G. B. & Field, R. W. Perspective: the first ten years of broadband chirped pulse Fourier transform microwave spectroscopy. *J. Chem. Phys.* **144**, 200901 (2016).
- Xie, F. et al. Discovering the elusive global minimum in a ternary chiral cluster: rotational spectra of propylene oxide trimer. *Angew. Chem. Int. Ed.* **59**, 22427–22430 (2020).
- Wang, J. et al. The unexplored world of cycloalkene–water complexes: primary and assisting interactions unraveled by experimental and computational spectroscopy. *Angew. Chem. Int. Ed.* **58**, 13935–13941 (2019).
- Alonso, J. L. & López, J. C. in *Gas-Phase IR Spectroscopy and Structure of Biological Molecules* (eds Rijss, A. M. & Oomens, J.) 335–401 (Springer International, 2015).
- Atanasov, M. et al. First principles approach to the electronic structure, magnetic anisotropy and spin relaxation in mononuclear 3d-transition metal single molecule magnets. *Coord. Chem. Rev.* **289–290**, 177–214 (2015).
- Barone, V. in *Computational Strategies for Spectroscopy: From Small Molecules to Nano Systems* (Wiley, 2011).
- Grunberg, J. in *Computational Spectroscopy: Methods, Experiments and Applications* (Wiley, 2011).
- Jensen, P., Bunker, P. R. in *Computational Molecular Spectroscopy* (Wiley, 2000).
- Neese, F. Prediction of molecular properties and molecular spectroscopy with density functional theory: from fundamental theory to exchange-coupling. *Coord. Chem. Rev.* **253**, 526–563 (2009).
- Neese, F., Petrenko, T., Ganyushin, D. & Olbrich, G. Advanced aspects of ab initio theoretical optical spectroscopy of transition metal complexes: multiplets, spin–orbit coupling and resonance Raman intensities. *Coord. Chem. Rev.* **251**, 288–327 (2007). **This review reports a careful analysis of quantum-chemical approaches for the study of transition metal complexes.**
- Mata, R. A. & Suhm, M. A. Benchmarking quantum chemical methods: are we heading in the right direction? *Angew. Chem. Int. Ed.* **56**, 11011–11018 (2017).
- Born, M. & Oppenheimer, R. Zur quantentheorie der moleküle. *Ann. Phys.* **389**, 457–484 (1927).
- Eckart, C. Some studies concerning rotating axes and polyatomic molecules. *Phys. Rev.* **47**, 552–558 (1935).
- Sayvetz, A. The kinetic energy of polyatomic molecules. *J. Chem. Phys.* **7**, 383–389 (1939).
- Watson, J. K. G. Simplification of the molecular vibration–rotation Hamiltonian. *Mol. Phys.* **15**, 479–490 (1968).
- Watson, J. K. G. The vibration–rotation Hamiltonian of linear molecules. *Mol. Phys.* **19**, 465–487 (1970).
- Furtenbacher, T., Császár, A. G. & Tennyson, J. MARVEL: measured active rotational–vibrational energy levels. *J. Mol. Spectrosc.* **245**, 115–125 (2007).
- Furtenbacher, T. & Császár, A. G. On employing H<sub>2</sub><sup>16</sup>O, H<sub>2</sub><sup>17</sup>O, H<sub>2</sub><sup>18</sup>O, and D<sub>2</sub><sup>16</sup>O lines as frequency standards in the 15–170 cm<sup>-1</sup> window. *J. Quant. Spectrosc. Radiat. Transfer* **109**, 1234–1251 (2008).
- Aliev, M. R. & Watson, J. K. G. in *Molecular Spectroscopy: Modern Research* (ed. Narahari Rao, K.) 1–67 (Academic, 1985). **This book presents the higher-order effects in the vibration–rotation spectra of semi-rigid molecules.**
- Gordy, W. & Cook, R. L. in *Microwave Molecular Spectra* (ed. Weissberger, A.) (Wiley, 1984).
- Watson, J. K. G. in *Vibrational Spectra and Structure: A Series of Advances* (ed. Durig, J. R.) (Elsevier, 1977).
- Kaupp, M., Buhl, M. & Malkin, V. G. in *Calculation of NMR and EPR Parameters. Theory and Applications* (eds Kaupp, M., Buhl, M. & Malkin, V. G.) (Wiley, 2004).
- Barone, V. & Polimeno, A. in *Electron Paramagnetic Resonance: A Practitioner's Toolkit* Ch. 7 (eds Brustolon, M. & Giambello, E.) 251–284 (Wiley, 2008).
- Jose, K. V. & Raghavachari, K. Fragment-based approach for the evaluation of NMR chemical shifts

- for large biomolecules incorporating the effects of the solvent environment. *J. Chem. Theory Comput.* **13**, 1147–1158 (2017).
33. Neese, F. Quantum chemistry and EPR parameters. *eMagRes* **6**, 1–22 (2017). **This article presents a recent and exhaustive review on the quantum-chemical computation of the parameters involved in the electron paramagnetic resonance spectroscopy.**
34. Puzzarini, C., Bloino, J., Tasinato, N. & Barone, V. Accuracy and interpretability: the Devil and the Holy Grail. New routes across old boundaries in computational spectroscopy. *Chem. Rev.* **119**, 8131–8191 (2019). **This recent review on computational (rotational and vibrational) spectroscopy also addresses accuracy and interpretability challenges.**
35. Bloino, J., Biczysko, M. & Barone, V. Anharmonic effects on vibrational spectra intensities: infrared, Raman, vibrational circular dichroism, and raman optical activity. *J. Phys. Chem. A* **119**, 11862–11874 (2015).
36. Nielsen, H. H. The vibration–rotation energies of molecules. *Rev. Mod. Phys.* **23**, 90–136 (1951).
37. Mills, I. A. in *Molecular Spectroscopy: Modern Research* (eds Rao, K. N. & Mathews, C. N.) (Academic, 1972).
38. Barone, V. Anharmonic vibrational properties by a fully automated second-order perturbative approach. *J. Chem. Phys.* **122**, 14108 (2005).
39. Bloino, J. & Barone, V. A second-order perturbation theory route to vibrational averages and transition properties of molecules: general formulation and application to infrared and vibrational circular dichroism spectroscopies. *J. Chem. Phys.* **136**, 124108 (2012).
40. Vázquez, J. & Stanton, J. F. Simple(r) algebraic equation for transition moments of fundamental transitions in vibrational second-order perturbation theory. *Mol. Phys.* **104**, 377–388 (2006).
41. Willetts, A., Handy, N. C., Green, W. H. & Jayatilaka, D. Anharmonic corrections to vibrational transition intensities. *J. Phys. Chem.* **94**, 5608–5616 (1990).
42. Császár, A. G. Anharmonic molecular force fields. *WIREs Comput. Mol. Sci.* **2**, 273–289 (2012).
43. Franke, P. R., Stanton, J. F. & Douberry, G. E. How to VPT2: accurate and intuitive simulations of CH stretching infrared spectra using VPT2+K with large effective Hamiltonian resonance treatments. *J. Phys. Chem. A* **125**, 1301–1324 (2021). **This recent and instructive review on vibrational perturbation theory also discusses in detail the treatment of resonances.**
44. Cornaton, Y., Ringholm, M., Louant, O. & Ruud, K. Analytic calculations of anharmonic infrared and Raman vibrational spectra. *Phys. Chem. Chem. Phys.* **18**, 4201–4215 (2016).
45. Maslen, P. E., Jayatilaka, D., Colwell, S. M., Amos, R. D. & Handy, N. C. Higher analytic derivatives. II. The fourth derivative of self-consistent-field energy. *J. Chem. Phys.* **95**, 7409–7417 (1991).
46. Piccardo, M., Bloino, J. & Barone, V. Generalized vibrational perturbation theory for rovibrational energies of linear, symmetric and asymmetric tops: theory, approximations, and automated approaches to deal with medium-to-large molecular systems. *Int. J. Quantum Chem.* **115**, 948–982 (2015).
47. Roy, T. K. & Gerber, R. B. Vibrational self-consistent field calculations for spectroscopy of biological molecules: new algorithmic developments and applications. *Phys. Chem. Chem. Phys.* **15**, 9468–9492 (2013).
48. Neff, M. & Rauhut, G. Toward large scale vibrational configuration interaction calculations. *J. Chem. Phys.* **131**, 124129 (2009).
49. Christiansen, O. Vibrational coupled cluster theory. *J. Chem. Phys.* **120**, 2149–2159 (2004).
50. Erfort, S., Tschope, M. & Rauhut, G. Toward a fully automated calculation of rovibrational infrared intensities for semi-rigid polyatomic molecules. *J. Chem. Phys.* **152**, 244104 (2020).
51. Biczysko, M., Bloino, J., Santoro, F. & Barone, V. in *Computational Strategies for Spectroscopy: From Small Molecules to Nano Systems* Ch. 8 (ed. Barone, V.) 361–443 (Wiley, 2011).
52. Bloino, J., Biczysko, M., Santoro, F. & Barone, V. General approach to compute vibrationally resolved one-photon electronic spectra. *J. Chem. Theory Comput.* **6**, 1256–1274 (2010).
53. Baiardi, A., Bloino, J. & Barone, V. General time dependent approach to vibronic spectroscopy including Franck–Condon, Herzberg–Teller, and Duschinsky effects. *J. Chem. Theory Comput.* **9**, 4097–4115 (2013).
54. Franck, J. & Dymond, E. G. Elementary processes of photochemical reactions. *Trans. Faraday Society* **21**, 536–542 (1926).
55. Condon, E. U. Nuclear motions associated with electron transitions in diatomic molecules. *Phys. Rev.* **32**, 858–872 (1928).
56. Herzberg, G. & Teller, E. Schwingungsstruktur der Elektronenübergänge bei mehratomigen Molekülen. *Z. Phys. Chem.* **21B**, 410–446 (1933).
57. Duschinsky, F. *Acta Physicochim.* **7**, 551–566 (URSS, 1937).
58. Baiardi, A., Bloino, J. & Barone, V. General formulation of vibronic spectroscopy in internal coordinates. *J. Chem. Phys.* **144**, 084114 (2016).
59. Reimers, J. R. A practical method for the use of curvilinear coordinates in calculations of normal-mode-projected displacements and Duschinsky rotation matrices for large molecules. *J. Chem. Phys.* **115**, 9103–9109 (2001).
60. Baiardi, A., Bloino, J. & Barone, V. Simulation of vibronic spectra of flexible systems: hybrid DVR-harmonic approaches. *J. Chem. Theory Comput.* **13**, 2804–2822 (2017).
61. Barone, V. The virtual multifrequency spectrometer: a new paradigm for spectroscopy. *Wiley Interdiscip. Rev. Comput. Mol. Sci.* **6**, 86–110 (2016). **This review introduces a new and more intuitive approach of computational spectroscopy based on the vis-à-vis comparison of calculated and experimental spectra instead of the mere computation of spectroscopic parameters.**
62. Bloino, J., Baiardi, A. & Biczysko, M. Aiming at an accurate prediction of vibrational and electronic spectra for medium-to-large molecules: an overview. *Int. J. Quantum Chem.* **116**, 1543–1574 (2016). **This tutorial review presents a detailed computational protocol and guidelines for the simulation of vibrational and vibrationally resolved electronic spectra for medium to large molecular systems of increasing flexibility.**
63. Autschbach, J. in *Comprehensive Chiroptical Spectroscopy: Instrumentation, Methodologies, and Theoretical Simulations* Vol. 1 Ch. 21 (eds Berova, N., Polavarapu, P. L., Nakanishi, K. & Woody, R. W.) 593–642 (Wiley, 2011).
64. Crawford, T. D. in *Comprehensive Chiroptical Spectroscopy: Instrumentation, Methodologies, and Theoretical Simulations* Vol. 1 Ch. 23 (eds Berova, N., Polavarapu, P. L., Nakanishi, K. & Woody, R. W.) 675–697 (Wiley, 2011).
65. Srebro-Hooper, M. & Autschbach, J. Calculating natural optical activity of molecules from first principles. *Annu. Rev. Phys. Chem.* **68**, 399–420 (2017). **This recent review outlines computational models and methodological developments for chiroptical spectroscopic methods that include optical rotation, ECD, VCD and ROA.**
66. Stephens, P. J., Devlin, F. J. & Cheeseman, J. R. in *VCD Spectroscopy for Organic Chemists* (CRC, 2012).
67. Ruud, K. in *Comprehensive Chiroptical Spectroscopy: Instrumentation, Methodologies, and Theoretical Simulations* Vol. 1 Ch. 24 (eds Berova, N., Polavarapu, P. L., Nakanishi, K. & Woody, R. W.) 699–727 (Wiley, 2011).
68. Beer, A. Bestimmung der absorption des rothen lichts in farbigen flüssigkeiten. *Ann. Phys.* **162**, 78–88 (1852).
69. Polavarapu, P. L. in *Chiroptical Spectroscopy: Fundamentals and Applications* (CRC, 2016).
70. Stephens, P. J. & Harada, N. ECD cotton effect approximated by the Gaussian curve and other methods. *Chirality* **22**, 229–233 (2010).
71. Cheeseman, J. R. & Frisch, M. J. Basis set dependence of vibrational Raman and Raman optical activity intensities. *J. Chem. Theory Comput.* **7**, 3323–3334 (2011).
72. Liégeois, V., Ruud, K. & Champagne, B. An analytical derivative procedure for the calculation of vibrational Raman optical activity spectra. *J. Chem. Phys.* **127**, 204105 (2007).
73. Nafie, L. A. Theory of Raman scattering and Raman optical activity: near resonance theory and levels of approximation. *Theor. Chem. Acc.* **119**, 39–55 (2008).
74. Barron, L. D. in *Molecular Light Scattering and Optical Activity* (Cambridge Univ. Press, Cambridge, 2004).
75. Long, D. A. in *The Raman Effect: A Unified Treatment of the Theory of Raman Scattering by Molecules* (Wiley, 2002).
76. Neugebauer, J., Reiher, M., Kind, C. & Hess, B. A. Quantum chemical calculation of vibrational spectra of large molecules—Raman and IR spectra for Buckminsterfullerene. *J. Comput. Chem.* **23**, 895–910 (2002).
77. Dzigan, L. C., DiRisio, R. J., Madison, L. R. & McCoy, A. B. Spectral signatures of proton delocalization in  $H\cdot(H_2O)_{n=1-4}$  ions. *Faraday Discuss.* **212**, 443–466 (2018).
78. Tanaka, S., Roy, P.-N. & Mitas, L. in *Recent progress in Quantum Monte Carlo Vol. 1234* (ACS, 2016).
79. Tanaka, S., Rothstein, S. M. & Lester Jr, W. A. in *Advances in Quantum Monte Carlo Vol. 1094* (ACS, 2012).
80. Anderson, J. B. & Rothstein, S. M. in *Advances in Quantum Monte Carlo Vol. 953* (ACS, 2007).
81. Lester, W. A., Rothstein, S. M. & Tanaka, S. in *Recent Advances in Quantum Monte Carlo Methods: Part II Recent Advances in Computational Chemistry Vol. 2* (World Scientific, 2002).
82. Lester, W. A., Rothstein, S. M. & Tanaka, S. in *Recent Advances in Quantum Monte Carlo Methods Recent Advances in Computational Chemistry* (World Scientific, 1997).
83. McCoy, A. B. Diffusion Monte Carlo approaches for investigating the structure and vibrational spectra of fluxional systems. *Int. Rev. Phys. Chem.* **25**, 77–107 (2006).
84. Suhm, M. A. & Watts, R. O. Quantum Monte Carlo studies of vibrational states in molecules and clusters. *Phys. Rep.* **204**, 293–329 (1991). **This article presents an extensive review of the DMC approach and its application to the studies of nuclear quantum effects in molecules and clusters.**
85. Anderson, J. B. A random-walk simulation of the Schrödinger equation:  $H^{1,5}$ . *J. Chem. Phys.* **63**, 1499–1503 (1975). **This key publication introduces the DMC approaches described in this Primer to the chemistry community.**
86. Anderson, J. B. Quantum chemistry by random walk.  $H^{2P}, H^{1,5}D_{3h}|A'_1, H_2|^{2S+u}, H_4|^{1\Sigma^+}, Be|^{1S}$ . *J. Chem. Phys.* **65**, 4121–4127 (1976).
87. Barnett, R. N., Reynolds, P. J. & Lester, W. A. Monte Carlo algorithms for expectation values of coordinate operators. *J. Comput. Phys.* **96**, 258–276 (1991).
88. Petit, A. S., Wellen, B. A. & McCoy, A. B. Using fixed-node diffusion Monte Carlo to investigate the effects of rotation-vibration coupling in highly fluxional asymmetric top molecules: application to  $H_2D^+$ . *J. Chem. Phys.* **138**, 034105 (2013).
89. Lee, H.-S., Herbert, J. M. & McCoy, A. B. Adiabatic diffusion Monte Carlo approaches for studies of ground and excited state properties of van der Waals complexes. *J. Chem. Phys.* **110**, 5481–5484 (1999).
90. Császár, A. G., Allen, W. D. & Schaefer III, H. F. In pursuit of the ab initio limit for conformational energy prototypes. *J. Chem. Phys.* **108**, 9751–9764 (1998).
91. Montgomery, J. A., Frisch, M. J., Ochterski, J. W. & Petersson, G. A. A complete basis set model chemistry. VI. Use of density functional geometries and frequencies. *J. Chem. Phys.* **110**, 2822–2827 (1999).
92. Demaison, J., Margules, L. & Boggs, J. E. The equilibrium C–Cl, C–Br, and C–I bond lengths from ab initio calculations, microwave and infrared spectroscopies, and empirical correlations. *Struct. Chem.* **14**, 159–174 (2003).
93. Puzzarini, C. Extrapolation to the complete basis set limit of structural parameters: comparison of different approaches. *J. Phys. Chem. A* **113**, 14530–14535 (2009).
94. Puzzarini, C. & Barone, V. Extending the molecular size in accurate quantum-chemical calculations: the equilibrium structure and spectroscopic properties of uracil. *Phys. Chem. Chem. Phys.* **13**, 7189–7197 (2011).
95. Alessandri, S., Barone, V. & Puzzarini, C. Extension of the “cheap” composite approach to noncovalent interactions: the jun–ChS scheme. *J. Chem. Theory Comput.* **16**, 988–1006 (2020).
96. Tajti, A. et al. HEAT: high accuracy extrapolated ab initio thermochemistry. *J. Chem. Phys.* **121**, 11599–11613 (2004).
97. Heckert, M., Kállay, M., Tew, D. P., Klopper, W. & Gauss, J. Basis-set extrapolation techniques for the accurate calculation of molecular equilibrium geometries using coupled-cluster theory. *J. Chem. Phys.* **125**, 044108 (2006).
98. Puzzarini, C., Heckert, M. & Gauss, J. The accuracy of rotational constants predicted by high-level quantum-chemical calculations. I. Molecules

- containing first-row atoms. *J. Chem. Phys.* **128**, 194108 (2008).
99. Yu, Q. et al. Structure, anharmonic vibrational frequencies, and intensities of NNNNN<sup>+</sup>. *J. Phys. Chem. A* **119**, 11623–11631 (2015).
  100. Boese, A. D. et al. W3 theory: robust computational thermochemistry in the kJ/mol accuracy range. *J. Chem. Phys.* **120**, 4129–4141 (2004).
  101. Karton, A., Rabinovich, E., Martin, J. M. L. & Ruscic, B. W4 theory for computational thermochemistry: in pursuit of confident sub-kJ/mol predictions. *J. Chem. Phys.* **125**, 144108 (2006).
  102. Peterson, K. A., Feller, D. & Dixon, D. A. Chemical accuracy in ab initio thermochemistry and spectroscopy: current strategies and future challenges. *Theor. Chem. Acc.* **131**, 1079 (2012).
  103. Shavitt, I. & Bartlett, R. J. in *Many-Body Methods in Chemistry and Physics: MBPT and Coupled-Cluster Theory* Cambridge Molecular Science (Cambridge Univ. Press, 2009).
  104. Raghavachari, K., Trucks, G. W., Pople, J. A. & Head-Gordon, M. A fifth-order perturbation comparison of electron correlation theories. *Chem. Phys. Lett.* **589**, 37–40 (2013).
  105. Kong, L., Bischoff, F. A. & Valeev, E. F. Explicitly correlated R12/F12 methods for electronic structure. *Chem. Rev.* **112**, 75–107 (2012).
  106. Neese, F., Hansen, A. & Liakos, D. G. Efficient and accurate approximations to the local coupled cluster singles doubles method using a truncated pair natural orbital basis set. *J. Chem. Phys.* **131**, 064103 (2009).
  107. Neese, F., Wennmohs, F. & Hansen, A. Efficient and accurate local approximations to coupled-electron pair approaches: an attempt to revive the pair natural orbital method. *J. Chem. Phys.* **130**, 114108 (2009). **This key publication reports the development and validation of an approach to extend the application of accurate quantum-chemical methods to large molecular systems.**
  108. Becke, A. D. Density-functional thermochemistry. III. The role of exact exchange. *J. Chem. Phys.* **98**, 5648–5652 (1993).
  109. Lee, C., Yang, W. & Parr, R. G. Development of the Colle–Salvetti correlation-energy formula into a functional of the electron density. *Phys. Rev. B* **37**, 785–789 (1988).
  110. Grimme, S. Semiempirical hybrid density functional with perturbative second-order correlation. *J. Chem. Phys.* **124**, 034108 (2006). **This key publication reports the introduction of double-hybrid functionals allowing quantitative spectroscopic studies by DFT.**
  111. Möller, C. & Plesset, M. S. Note on an approximation treatment for many-electron systems. *Phys. Rev.* **46**, 618–622 (1934).
  112. Barone, V., Biczysko, M., Bloino, J. & Puzzarini, C. Accurate molecular structures and infrared spectra of *trans*-2,3-dideuterooxirane, methyloxirane, and *trans*-2,3-dimethyloxirane. *J. Chem. Phys.* **141**, 034107 (2014).
  113. Barone, V., Biczysko, M., Bloino, J. & Puzzarini, C. Accurate structure, thermodynamic and spectroscopic parameters from CC and CC/DFT schemes: the challenge of the conformational equilibrium in glycine. *Phys. Chem. Chem. Phys.* **15**, 10094–10111 (2013).
  114. Jurečka, P., Šponer, J., Černý, J. & Hobza, P. Benchmark database of accurate (MP2 and CCSD(T) complete basis set limit) interaction energies of small model complexes, DNA base pairs, and amino acid pairs. *Phys. Chem. Chem. Phys.* **8**, 1985–1993 (2006).
  115. Režáč, J., Riley, K. E. & Hobza, P. S66: a well-balanced database of benchmark interaction energies relevant to biomolecular structures. *J. Chem. Theory Comput.* **7**, 2427–2438 (2011).
  116. Režáč, J., Bím, D., Gutten, O. & Rulíšek, L. Toward accurate conformational energies of smaller peptides and medium-sized macrocycles: MPCONF196 benchmark energy data set. *J. Chem. Theory Comput.* **14**, 1254–1266 (2018).
  117. Goerigk, L. et al. A look at the density functional theory zoo with the advanced GMTKN55 database for general main group thermochemistry, kinetics and noncovalent interactions. *Phys. Chem. Chem. Phys.* **19**, 32184–32215 (2017).
  118. Biczysko, M., Panek, P., Scalmani, G., Bloino, J. & Barone, V. Harmonic and anharmonic vibrational frequency calculations with the double-hybrid B2PLYP method: analytic second derivatives and benchmark studies. *J. Chem. Theory Comput.* **6**, 2115–2125 (2010).
  119. Barone, V., Biczysko, M. & Bloino, J. Fully anharmonic IR and Raman spectra of medium-size molecular systems: accuracy and interpretation. *Phys. Chem. Chem. Phys.* **16**, 1759–1787 (2014).
  120. Shu, C., Jiang, Z. & Biczysko, M. Toward accurate prediction of amino acid derivatives structure and energetics from DFT: glycine conformers and their interconversions. *J. Mol. Model.* **26**, 129 (2020).
  121. Brémond, É. et al. Benchmarking density functionals on structural parameters of small-/medium-sized organic molecules. *J. Chem. Theory Comput.* **12**, 459–465 (2016).
  122. Risthaus, T., Steinmetz, M. & Grimme, S. Implementation of nuclear gradients of range-separated hybrid density functionals and benchmarking on rotational constants for organic molecules. *J. Comput. Chem.* **35**, 1509–1516 (2014).
  123. Su, N. Q. & Xu, X. Beyond energies: geometry predictions with the XYG3 type of doubly hybrid density functionals. *Chem. Commun.* **52**, 13840–13860 (2016).
  124. Witte, J., Goldey, M., Neaton, J. B. & Head-Gordon, M. Beyond energies: geometries of nonbonded molecular complexes as metrics for assessing electronic structure approaches. *J. Chem. Theory Comput.* **11**, 1481–1492 (2015).
  125. Yu, H. S., He, X., Li, S. L. & Truhlar, D. G. MN15: a Kohn–Sham global-hybrid exchange–correlation density functional with broad accuracy for multi-reference and single-reference systems and noncovalent interactions. *Chem. Sci.* **7**, 5032–5051 (2016).
  126. Bousselli, R., Ceselin, G., Tasinato, N. & Barone, V. DFT meets the segmented polarization consistent basis sets: performances in the computation of molecular structures, rotational and vibrational spectroscopic properties. *J. Mol. Struct.* **1208**, 127886 (2020).
  127. Hanson-Heine, M. W. D. Benchmarking DFT-D dispersion corrections for anharmonic vibrational frequencies and harmonic scaling factors. *J. Phys. Chem. A* **123**, 9800–9808 (2019).
  128. Loos, P.-F., Lipparini, F., Boggio-Pasqua, M., Scemama, A. & Jacquemin, D. A mountaineering strategy to excited states: highly accurate energies and benchmarks for medium sized molecules. *J. Chem. Theory Comput.* **16**, 1711–1741 (2020).
  129. Brémond, E., Savarese, M., Adamo, C. & Jacquemin, D. Accuracy of TD-DFT geometries: a fresh look. *J. Chem. Theory Comput.* **14**, 3715–3727 (2018).
  130. Egidi, F. et al. Effective inclusion of mechanical and electrical anharmonicity in excited electronic states: VPT2-TDDFT route. *J. Chem. Theory Comput.* **13**, 2789–2803 (2017).
  131. Bomble, Y. J. et al. Equation-of-motion coupled-cluster methods for ionized states with an approximate treatment of triple excitations. *J. Chem. Phys.* **122**, 154107 (2005).
  132. Roos, B. O., Lindh, R., Malmqvist, P. Å., Veryazov, V. & Widmark, P.-O. in *Multiconfigurational Quantum Chemistry* (Wiley, 2016).
  133. Auer, A. A. et al. A case study of density functional theory and domain-based local pair natural orbital coupled cluster for vibrational effects on EPR hyperfine coupling constants: vibrational perturbation theory versus ab initio molecular dynamics. *Mol. Phys.* **118**, e1797916 (2020).
  134. Datta, D., Saitow, M., Sandhöfer, B. & Neese, F. <sup>57</sup>Fe Mössbauer parameters from domain based local pair–natural orbital coupled-cluster theory. *J. Chem. Phys.* **153**, 204101 (2020).
  135. Sirohiwal, A., Berraud-Pache, R., Neese, F., Izsák, R. & Pantazis, D. A. Accurate computation of the absorption spectrum of chlorophyll a with pair natural orbital coupled cluster methods. *J. Phys. Chem. B* **124**, 8761–8771 (2020).
  136. Biaardi, A. & Reiher, M. The density matrix renormalization group in chemistry and molecular physics: recent developments and new challenges. *J. Chem. Phys.* **152**, 040903 (2020). **This review is the most recent on the use of methods rooted in the density matrix renormalization group for vibrational and electronic spectroscopy.**
  137. Andersson, K., Malmqvist, P. Å. & Roos, B. O. Second-order perturbation theory with a complete active space self-consistent field reference function. *J. Chem. Phys.* **96**, 1218–1226 (1992).
  138. Andersson, K., Malmqvist, P. A., Roos, B. O., Sadlej, A. J. & Wolinski, K. Second-order perturbation theory with a CASSCF reference function. *J. Phys. Chem.* **94**, 5483–5488 (1990).
  139. Angel, C., Cimiraglia, R., Evangelisti, S., Leininger, T. & Malrieu, J.-P. Introduction of *n*-electron valence states for multireference perturbation theory. *J. Chem. Phys.* **114**, 10252–10264 (2001).
  140. Puzzarini, C., Stanton, J. F. & Gauss, J. Quantum-chemical calculation of spectroscopic parameters for rotational spectroscopy. *Int. Rev. Phys. Chem.* **29**, 273–367 (2010). **This article presents an authoritative review on computational rotational spectroscopy.**
  141. Licari, D., Tasinato, N., Spada, L., Puzzarini, C. & Barone, V. VMS-ROT: a new module of the virtual multifrequency spectrometer for simulation, interpretation, and fitting of rotational spectra. *J. Chem. Theory Comput.* **13**, 4382–4396 (2017).
  142. Lesarri, A., Mata, S., López, J. C. & Alonso, J. L. A laser-ablation molecular-beam Fourier-transform microwave spectrometer: the rotational spectrum of organic solids. *Rev. Sci. Instrum.* **74**, 4799–4804 (2003).
  143. Mancini, G., Fusè, M., Lazzari, F., Chandramouli, B. & Barone, V. Unsupervised search of low-lying conformers with spectroscopic accuracy: a two-step algorithm rooted into the island model evolutionary algorithm. *J. Chem. Phys.* **153**, 124110 (2020).
  144. Császár, A. G. et al. The fourth age of quantum chemistry: molecules in motion. *Phys. Chem. Chem. Phys.* **14**, 1085–1106 (2012).
  145. Biaardi, A., Stein, C. J., Barone, V. & Reiher, M. Vibrational density matrix renormalization group. *J. Chem. Theory Comput.* **13**, 3764–3777 (2017).
  146. Carter, S., Sharma, A. R., Bowman, J. M., Rosmus, P. & Tarroni, R. Calculations of rovibrational energies and dipole transition intensities for polyatomic molecules using MULTIMODE. *J. Chem. Phys.* **131**, 224106 (2009).
  147. Begušić, T. & Vančiček, J. On-the-fly ab initio semiclassical evaluation of vibronic spectra at finite temperature. *J. Chem. Phys.* **153**, 024105 (2020).
  148. Hirshberg, B., Sagiv, L. & Gerber, R. B. Approximate quantum dynamics using ab initio classical separable potentials: spectroscopic applications. *J. Chem. Theory Comput.* **13**, 982–991 (2017).
  149. Gaigeot, M.-P. Theoretical spectroscopy of floppy peptides at room temperature. A DFTMD perspective: gas and aqueous phase. *Phys. Chem. Chem. Phys.* **12**, 3336–3359 (2010).
  150. Pracht, P., Bohle, F. & Grimme, S. Automated exploration of the low-energy chemical space with fast quantum chemical methods. *Phys. Chem. Chem. Phys.* **22**, 7169–7192 (2020).
  151. Del Galdo, S., Fusè, M. & Barone, V. The ONIOM/PMM model for effective yet accurate simulation of optical and chiroptical spectra in solution: camphorquinone in methanol as a case study. *J. Chem. Theory Comput.* **16**, 3294–3306 (2020).
  152. Panek, P. T. & Jacob, C. R. Anharmonic theoretical vibrational spectroscopy of polypeptides. *J. Phys. Chem. Lett.* **7**, 3084–3090 (2016).
  153. Roy, T. K., Sharma, R. & Gerber, R. B. First-principles anharmonic quantum calculations for peptide spectroscopy: VSCF calculations and comparison with experiments. *Phys. Chem. Chem. Phys.* **18**, 1607–1614 (2016).
  154. Barone, V., Imrota, R. & Rega, N. Quantum mechanical computations and spectroscopy: from small rigid molecules in the gas phase to large flexible molecules in solution. *Acc. Chem. Res.* **41**, 605–616 (2008).
  155. Balabin, R. M. Conformational equilibrium in glycine: focal-point analysis and ab initio limit. *Chem. Phys. Lett.* **479**, 195–200 (2009).
  156. Bazsó, G., Magyarfalvi, G. & Tarczay, G. Tunneling lifetime of the ttc/tp conformer of glycine in low-temperature matrices. *J. Phys. Chem. A* **116**, 10539–10547 (2012).
  157. Stepanian, S. G. et al. Matrix-isolation infrared and theoretical studies of the glycine conformers. *J. Phys. Chem. A* **102**, 1041–1054 (1998).
  158. Balabin, R. M. Conformational equilibrium in glycine: experimental jet-cooled Raman spectrum. *J. Phys. Chem. Lett.* **1**, 20–23 (2010).
  159. Lockyear, J. F. et al. Isomer specific product detection in the reaction of CH with acrolein. *J. Phys. Chem. A* **117**, 11013–11026 (2013).
  160. Barone, V., Biczysko, M., Borkowska-Panek, M. & Bloino, J. A multifrequency virtual spectrometer for complex bio-organic systems: vibronic and environmental effects on the UV/Vis spectrum of chlorophyll-a. *ChemPhysChem* **15**, 3355–3364 (2014).
  161. Gouterman, M. Spectra of porphyrins. *J. Mol. Spectrosc.* **6**, 138–163 (1961).

162. Rätsep, M. et al. Absorption-emission symmetry breaking and the different origins of vibrational structures of the  ${}^1\text{Q}_y$  and  ${}^1\text{Q}_x$  electronic transitions of pheophytin *a*. *J. Chem. Phys.* **151**, 165102 (2019).
163. Huang, X., Braams, B. J. & Bowman, J. M. Ab initio potential energy and dipole moment surfaces for  $\text{H}_2\text{O}_2^+$ . *J. Chem. Phys.* **122**, 044308 (2005).
164. Petit, A. S., Ford, J. E. & McCoy, A. B. Simultaneous evaluation of multiple rotationally excited states of  $\text{H}_3^+$ ,  $\text{H}_3\text{O}^+$ , and  $\text{CH}_5^+$  using diffusion Monte Carlo. *J. Phys. Chem. A* **118**, 7206–7220 (2014).
165. Petit, A. S. & McCoy, A. B. Diffusion Monte Carlo approaches for evaluating rotationally excited states of symmetric top molecules: application to  $\text{H}_2\text{O}^+$  and  $\text{D}_2\text{O}^+$ . *J. Phys. Chem. A* **113**, 12706–12714 (2009).
166. Sandler, P., Buch, V. & Clary, D. C. Calculation of expectation values of molecular systems using diffusion Monte Carlo in conjunction with the finite field method. *J. Chem. Phys.* **101**, 6353–6355 (1994).
167. Paesani, F. & Whaley, K. B. Rotational excitations of  $\text{N}_2\text{O}$  in small helium clusters and the role of Bose permutation symmetry. *J. Chem. Phys.* **121**, 5293–5311 (2004).
168. Cho, H. M. & Singer, S. J. Correlation function quantum Monte Carlo study of the excited vibrational states of  $\text{H}_2\text{O}_2^+$ . *J. Phys. Chem. A* **108**, 8691–8702 (2004).
169. McCoy, A. B., Diken, E. G. & Johnson, M. A. Generating spectra from ground-state wave functions: unraveling anharmonic effects in the  $\text{OH}^- \cdot \text{H}_2\text{O}$  vibrational predissociation spectrum. *J. Phys. Chem. A* **113**, 7346–7352 (2009).
170. Polavarapu, P. L. et al. A single chiroptical spectroscopic method may not be able to establish the absolute configurations of diastereomers: dimethylesters of hibiscus and garcinia acids. *J. Phys. Chem. A* **115**, 5665–5673 (2011).
171. Debie, E. et al. A confidence level algorithm for the determination of absolute configuration using vibrational circular dichroism or Raman optical activity. *ChemPhysChem* **12**, 1542–1549 (2011).
172. Fusè, M. et al. Unbiased determination of absolute configurations by vis-à-vis comparison of experimental and simulated spectra: the challenging case of diplopyrone. *J. Phys. Chem. B* **123**, 9230–9237 (2019).
173. Bogaerts, J. et al. A combined Raman optical activity and vibrational circular dichroism study on artemisinin-type products. *Phys. Chem. Chem. Phys.* **22**, 18014–18024 (2020). **This very recent study demonstrates the combined use of two chiroptical spectroscopic methods, VCD and ROA, in determining the absolute configuration of a molecule with seven chiral centres.**
174. Johnson, J. L. et al. Dissymmetry factor spectral analysis can provide useful diastereomer discrimination: chiral molecular structure of an analogue of (–)-cispine A. *ACS Omega* **4**, 6154–6164 (2019).
175. Hopmann, K. H. et al. Determining the absolute configuration of two marine compounds using vibrational chiroptical spectroscopy. *J. Org. Chem.* **77**, 858–869 (2012).
176. Covington, C. L. & Polavarapu, P. L. Similarity in dissymmetry factor spectra: a quantitative measure of comparison between experimental and predicted vibrational circular dichroism. *J. Phys. Chem. A* **117**, 3377–3386 (2013).
177. Nicu, V. P. & Baerends, E. J. Robust normal modes in vibrational circular dichroism spectra. *Phys. Chem. Chem. Phys.* **11**, 6107–6118 (2009).
178. Tommasini, M. et al. Mode robustness in Raman optical activity. *J. Chem. Theory Comput.* **10**, 5520–5527 (2014).
179. Freedman, T. B., Shih, M.-L., Lee, E. & Nafie, L. A. Electron transition current density in molecules. 3. Ab initio calculations for vibrational transitions in ethylene and formaldehyde. *J. Am. Chem. Soc.* **119**, 10620–10626 (1997).
180. Fusè, M., Egidi, F. & Bloino, J. Vibrational circular dichroism under the quantum magnifying glass: from the electronic flow to the spectroscopic observable. *Phys. Chem. Chem. Phys.* **21**, 4224–4239 (2019).
181. Hug, W. Visualizing Raman and Raman optical activity generation in polyatomic molecules. *Chem. Phys.* **264**, 53–69 (2001).
182. Yamamoto, S. in *Introduction to Astrochemistry: Chemical Evolution from Interstellar Clouds to Star and Planet Formation* (Springer, 2017).
183. Jørgensen, J. K., Belloche, A. & Garrod, R. T. Astrochemistry during the formation of stars. *Annu. Rev. Astron. Astrophys.* **58**, 727–778 (2020).
184. McGuire, B. A. 2018 census of interstellar, circumstellar, extragalactic, protoplanetary disk, and exoplanetary molecules. *Astrophys. J. Suppl. Ser.* **239**, 17 (2018).
185. Herbst, E. & van Dishoeck, E. F. Complex organic interstellar molecules. *Annu. Rev. Astron. Astrophys.* **47**, 427–480 (2009).
186. Lattelais, M., Pauzat, F., Ellinger, Y. & Ceccarelli, C. Interstellar complex organic molecules and the minimum energy principle. *Astrophys. J.* **696**, L133–L136 (2009).
187. Puzzarini, C. & Barone, V. A never-ending story in the sky: the secrets of chemical evolution. *Phys. Life Rev.* **32**, 59–94 (2020). **This recent review addresses the role of spectroscopic investigation for the characterization of molecules of astrochemical interest and their detection in space.**
188. Cernicharo, J., Guélin, M., Agúndez, M., McCarthy, M. C. & Thaddeus, P. Detection of  $\text{C}_5\text{N}^-$  and vibrationally excited  $\text{C}_2\text{H}$  in IRC+10216. *Astrophys. J.* **688**, L83–L86 (2008).
189. Botschwinia, P. & Oswald, R. Carbon chains of type  $\text{C}_{2n+1}\text{N}^-$  ( $n=2–6$ ): a theoretical study of potential interstellar anions. *J. Chem. Phys.* **129**, 044305 (2008).
190. Cazzoli, G., Cludi, L., Buffa, G. & Puzzarini, C. Precise THz measurements of  $\text{HCO}^+$ ,  $\text{N}_2\text{H}^+$  and  $\text{CF}^-$  for astrophysical observations. *Astrophys. J. Suppl. Ser.* **203**, 11 (2012).
191. Guzmán, V. et al. The hyperfine structure in the rotational spectrum of  $\text{CF}^-$ . *Astron. Astrophys.* **548**, A94 (2012).
192. Klos, J. & Lique, F. in *Cold Chemistry: Molecular Scattering and Reactivity Near Absolute Zero* Ch. 2 (eds Dulieu, O. & Osterwalder, A.) 46–91 (RSC, 2018).
193. Borrego-Villalas, R. et al. Two-dimensional UV spectroscopy: a new insight into the structure and dynamics of biomolecules. *Chem. Sci.* **10**, 9907–9921 (2019).
194. East, K. W. et al. NMR and computational methods for molecular resolution of allosteric pathways in enzyme complexes. *Biophys. Rev.* **12**, 155–174 (2020).
195. Huang, J., Zhou, Y. & Xie, D. Predicted infrared spectra in the HF stretching band of the  $\text{H}_2\text{-HF}$  complex. *J. Chem. Phys.* **149**, 094307 (2018).
196. Clary, D. C. & Nesbitt, D. J. Calculation of vibration-rotation spectra for rare gas–HCl complexes. *J. Chem. Phys.* **90**, 7000–7013 (1989).
197. Felker, P. M. & Bacic, Z.  $\text{H}_2\text{O}-\text{CO}$  and  $\text{D}_2\text{O}-\text{CO}$  complexes: intra- and intermolecular rovibrational states from full-dimensional and fully coupled quantum calculations. *J. Chem. Phys.* **153**, 074107 (2020).
198. Keutsch, F. N. & Saykally, R. J. Water clusters: untangling the mysteries of the liquid, one molecule at a time. *Proc. Natl Acad. Sci. USA.* **98**, 10533–10540 (2001). **This comprehensive review discusses how theory is used to predict and interpret experimental measurements of spectra for water clusters.**
199. Mukhopadhyay, A., Xantheas, S. S. & Saykally, R. J. The water dimer II: theoretical investigations. *Chem. Phys. Lett.* **700**, 163–175 (2018).
200. Schwan, R. et al. Observation of the low-frequency spectrum of the water dimer as a sensitive test of the water dimer potential and dipole moment surfaces. *Angew. Chem. Int. Ed.* **58**, 13119–13126 (2019).
201. Cisneros, G. A. et al. Modeling molecular interactions in water: from pairwise to many-body potential energy functions. *Chem. Rev.* **116**, 7501–7528 (2016).
202. Mallory, J. D. & Mandelshtam, V. A. Diffusion Monte Carlo studies of MB-pol ( $\text{H}_2\text{O}$ )<sub>2–6</sub> and ( $\text{D}_2\text{O}$ )<sub>2–6</sub> clusters: structures and binding energies. *J. Chem. Phys.* **145**, 064308 (2016).
203. Liu, K. et al. Characterization of a cage form of the water hexamer. *Nature* **381**, 501–503 (1996).
204. Lee, V. G. M., Vetterli, N. J., Boyer, M. A. & McCoy, A. B. Diffusion Monte Carlo studies on the detection of structural changes in the water hexamer upon isotopic substitution. *J. Phys. Chem. A* **124**, 6903–6912 (2020).
205. Richardson, J. O. et al. Concerted hydrogen-bond breaking by quantum tunneling in the water hexamer prism. *Science* **351**, 1310–1313 (2016).
206. Vaillant, C. L., Wales, D. J. & Althorpe, S. C. Tunneling splittings in water clusters from path integral molecular dynamics. *J. Phys. Chem. Lett.* **10**, 7300–7304 (2019).
207. Gaigeot, M. P. Unravelling the conformational dynamics of the aqueous alanine dipeptide with first-principle molecular dynamics. *J. Phys. Chem. B* **113**, 10059–10062 (2009).
208. Clary, D. C., Benoit, D. M. & van Mourik, T. H-Densities: a new concept for hydrated molecules. *Acc. Chem. Res.* **33**, 441–447 (2000).
209. Fornaro, T., Burini, D., Biczysko, M. & Barone, V. Hydrogen-bonding effects on infrared spectra from anharmonic computations: uracil–water complexes and uracil dimers. *J. Phys. Chem. A* **119**, 4224–4236 (2015).
210. Bec, K. B. & Huck, C. W. Breakthrough potential in near-infrared spectroscopy: spectra simulation, a review of recent developments. *Front. Chem.* **7**, 48 (2019). **This article presents a detailed review on the computational methods used for calculating the near infrared spectra of larger polyatomic molecules.**
211. Benoit, D. M. Rationalising the vibrational spectra of biomolecules using atomistic simulations. *Front. Biosci.* **14**, 4229–4241 (2009).
212. Bec, K. B., Grabska, J., Ozaki, Y., Czarnecki, M. A. & Huck, C. W. Simulated NIR spectra as sensitive markers of the structure and interactions in nucleobases. *Sci. Rep.* **9**, 17398 (2019).
213. Atanasov, M., Ganushkin, D., Sivalingam, K. & Neese, F. in *Molecular Electronic Structures of Transition Metal Complexes II* Ch. 6 (eds Mingso, D. M. P., Day, P. & Dahl, J. P.) 149–220 (Springer, 2012).
214. Singh, S. K., Atanasov, M. & Neese, F. Challenges in multireference perturbation theory for the calculations of the  $g$ -tensor of first-row transition-metal complexes. *J. Chem. Theory Comput.* **14**, 4662–4677 (2018).
215. Maganas, D. et al. First principles calculations of the structure and V L-edge X-ray absorption spectra of  $\text{V}_2\text{O}_5$  using local pair natural orbital coupled cluster theory and spin-orbit coupled configuration interaction approaches. *Phys. Chem. Chem. Phys.* **15**, 7260–7276 (2013).
216. Roemelt, M., Maganas, D., DeBeer, S. & Neese, F. A combined DFT and restricted open-shell configuration interaction method including spin-orbit coupling: application to transition metal L-edge X-ray absorption spectroscopy. *J. Chem. Phys.* **138**, 204101 (2013).
217. Neese, F. A critical evaluation of DFT, including time-dependent DFT, applied to bioinorganic chemistry. *J. Biol. Inorg. Chem.* **11**, 702–711 (2006).
218. Neese, F. High-level spectroscopy, quantum chemistry, and catalysis: not just a passing fad. *Angew. Chem. Int. Ed.* **56**, 11003–11010 (2017).
219. Neese, F., Atanasov, M., Bistoni, G., Maganas, D. & Ye, S. Chemistry and quantum mechanics in 2019: give us insight and numbers. *J. Am. Chem. Soc.* **141**, 2814–2824 (2019).
220. Zadrozny, J. M. & Long, J. R. Slow magnetic relaxation at zero field in the tetrahedral complex  $[\text{Co}(\text{SPH})_4]^{2-}$ . *J. Am. Chem. Soc.* **133**, 20732–20734 (2011).
221. Neese, F. & Pantazis, D. A. What is not required to make a single molecule magnet. *Faraday Discuss.* **148**, 229–238 (2011).
222. Suturina, E. A. et al. Magneto-structural correlations in pseudotetrahedral forms of the  $[\text{Co}(\text{SPH})_4]^{2-}$  complex probed by magnetometry, MCD spectroscopy, advanced EPR techniques, and ab initio electronic structure calculations. *Inorg. Chem.* **56**, 3102–3118 (2017).
223. Suturina, E. A., Maganas, D., Bill, E., Atanasov, M. & Neese, F. Magneto-structural correlations in a series of pseudotetrahedral  $[\text{Co}^{\text{II}}(\text{XR})_4]^{2-}$  single molecule magnets: an ab initio ligand field study. *Inorg. Chem.* **54**, 9948–9961 (2015).
224. Reckhemmer, Y. et al. A four-coordinate Cobalt(II) single-ion magnet with coercivity and a very high energy barrier. *Nat. Commun.* **7**, 10467 (2016).
225. Penocchio, E., Piccardo, M. & Barone, V. Semieperimental equilibrium structures for building blocks of organic and biological molecules: the B2PLY Route. *J. Chem. Theory Comput.* **11**, 4689–4707 (2015).
226. Kodrycka, M. & Patkowski, K. Platinum, gold, and silver standards of intermolecular interaction energy calculations. *J. Chem. Phys.* **151**, 070901 (2019).
227. Alessandrini, S., Gauss, J. & Puzzarini, C. Accuracy of rotational parameters predicted by high-level quantum-chemical calculations: case study of sulfur-containing molecules of astrochemical interest. *J. Chem. Theory Comput.* **14**, 5360–5371 (2018).
228. Dral, P. O. Quantum chemistry in the age of machine learning. *J. Phys. Chem. Lett.* **11**, 2336–2347 (2020). **This article is a general introduction on the use of machine learning in quantum chemistry.**

229. Liakos, D. G., Guo, Y. & Neese, F. Comprehensive benchmark results for the domain based local pair natural orbital coupled cluster method (DLPNO-CCSD(T)) for closed- and open-shell systems. *J. Phys. Chem. A* **124**, 90–100 (2020).
230. Nagy, P. R. & Kállay, M. Approaching the basis set limit of CCSD(T) energies for large molecules with local natural orbital coupled-cluster methods. *J. Chem. Theory Comput.* **15**, 5275–5298 (2019).
231. Sibert III, E. L. Modeling vibrational anharmonicity in infrared spectra of high frequency vibrations of polyatomic molecules. *J. Chem. Phys.* **150**, 090901 (2019).
232. Basdogan, Y. et al. Machine learning-guided approach for studying solvation environments. *J. Chem. Theory Comput.* **16**, 633–642 (2020).
233. Hodecker, M., Biczysko, M., Dreuw, A. & Barone, V. Simulation of vacuum UV absorption and electronic circular dichroism spectra of methyl oxirane: the role of vibrational effects. *J. Chem. Theory Comput.* **12**, 2820–2833 (2016).
234. Puzzarini, C., Biczysko, M., Bloino, J. & Barone, V. Accurate spectroscopic characterization of oxirane: a valuable route to its identification in Titan's atmosphere and the assignment of unidentified infrared bands. *Astrophys. J.* **785**, 107 (2014).
235. Karton, A., Sylvestsky, N. & Martin, J. M. L. W4-17: a diverse and high-confidence dataset of atomization energies for benchmarking high-level electronic structure methods. *J. Comput. Chem.* **38**, 2063–2075 (2017).
236. Mayhall, N. J. & Raghavachari, K. Molecules-in-molecules: an extrapolated fragment-based approach for accurate calculations on large molecules and materials. *J. Chem. Theory Comput.* **7**, 1336–1343 (2011).
237. Santra, G., Sylvestsky, N. & Martin, J. M. L. Minimally empirical double-hybrid functionals trained against the GMTKN55 database: revDSD-PBEP86-D4, revDOD-PBE-D4, and DOD-SCAN-D4. *J. Phys. Chem. A* **123**, 5129–5143 (2019).
238. Kussmann, J. & Ochsenfeld, C. Preselective screening for linear-scaling exact exchange-gradient calculations for graphics processing units and general strong-scaling massively parallel calculations. *J. Chem. Theory Comput.* **11**, 918–922 (2015).
239. Doser, B., Lambrecht, D. S. & Ochsenfeld, C. Tighter multipole-based integral estimates and parallel implementation of linear-scaling AO-MP2 theory. *Phys. Chem. Chem. Phys.* **10**, 3335–3344 (2008).
240. Ma, Q. & Werner, H.-J. Scalable electron correlation methods. 7. Local open-shell coupled-cluster methods using pair natural orbitals: PNO-RCCSD and PNO-UCCSD. *J. Chem. Theory Comput.* **16**, 3135–3151 (2020).
241. Becca, F. & Sorella, S. in *Quantum Monte Carlo Approaches for Correlated Systems* (Cambridge Univ. Press, 2017).
242. Puzzarini, C. & Barone, V. The challenging playground of astrochemistry: an integrated rotational spectroscopy—quantum chemistry strategy. *Phys. Chem. Chem. Phys.* **22**, 6507–6523 (2020).
243. Biczysko, M., Krupa, J. & Wierzejewska, M. Theoretical studies of atmospheric molecular complexes interacting with NIR to UV light. *Faraday Discuss.* **212**, 421–441 (2018).
244. Raucci, U. et al. Ab-initio molecular dynamics and hybrid explicit-implicit solvation model for aqueous and nonaqueous solvents: GFP chromophore in water and methanol solution as case study. *J. Comput. Chem.* **46**, 2228–2239 (2020).
245. Zhang, W., Kong, X., Liu, S. & Zhao, Y. Multi-coefficients correlation methods. *WIREs Comput. Mol. Sci.* **10**, e1474 (2020).
246. Gagliardi, L. et al. Multiconfiguration pair-density functional theory: a new way to treat strongly correlated systems. *Acc. Chem. Res.* **50**, 66–73 (2017).
247. Bannwarth, C. et al. Extended tight-binding quantum chemistry methods. *WIREs Comput. Mol. Sci.* **11**, e01493 (2020).
248. Loos, P.-F., Scemama, A. & Jacquemin, D. The quest for highly accurate excitation energies: a computational perspective. *J. Phys. Chem. Lett.* **11**, 2374–2383 (2020).
- This recent perspective article presents accurate computations of excitation energies.**
249. Casanova-Páez, M. & Goerigk, L. Assessing the Tamm–Dancoff approximation, singlet–singlet, and singlet–triplet excitations with the latest long-range corrected double-hybrid density functionals. *J. Chem. Phys.* **153**, 064106 (2020).
250. Mutter, S. T. et al. Conformational dynamics of carbohydrates: Raman optical activity of d-glucuronic acid and N-acetyl-d-glucosamine using a combined molecular dynamics and quantum chemical approach. *Phys. Chem. Chem. Phys.* **17**, 6016–6027 (2015).
251. Lee, V. G. M. & McCoy, A. B. An efficient approach for studies of water clusters using diffusion Monte Carlo. *J. Phys. Chem. A* **123**, 8063–8070 (2019).
252. Zhao, L. et al. Real-time time-dependent nuclear–electronic orbital approach: dynamics beyond the Born–Oppenheimer approximation. *J. Phys. Chem. Lett.* **11**, 4052–4058 (2020).
253. Petrenko, T. & Rauhut, G. A general approach for calculating strongly anharmonic vibronic spectra with a high density of states: the  $\tilde{X}^2\text{B}_1 \rightarrow \tilde{X}^1\text{A}_1$  photoelectron spectrum of difluoromethane. *J. Chem. Theory Comput.* **13**, 5515–5527 (2017).
254. Cerezo, J., Aranda, D., Avila Ferrer, F. J., Prampolini, G. & Santoro, F. Adiabatic-molecular dynamics generalized vertical hessian approach: a mixed quantum classical method to compute electronic spectra of flexible molecules in the condensed phase. *J. Chem. Theory Comput.* **16**, 1215–1231 (2020).
255. Jasper, A. W., Harding, L. B., Knight, C. & Georgievskii, Y. Anharmonic rovibrational partition functions at high temperatures: tests of reduced-dimensional models for systems with up to three fluxional modes. *J. Phys. Chem. A* **123**, 6210–6228 (2019).
256. Burd, T. A. H. & Clary, D. C. Analytic route to tunneling splittings using semiclassical perturbation theory. *J. Chem. Theory Comput.* **16**, 3486–3493 (2020).
257. O'Connor, M. B. et al. Interactive molecular dynamics in virtual reality from quantum chemistry to drug binding: an open-source multi-person framework. *J. Chem. Phys.* **150**, 220901 (2019).
258. McArdle, S., Endo, S., Aspuru-Guzik, A., Benjamin, S. C. & Yuan, X. Quantum computational chemistry. *Rev. Mod. Phys.* **92**, 015003 (2020).
259. Barone, V. et al. Implementation and validation of a multi-purpose virtual spectrometer for large systems in complex environments. *Phys. Chem. Chem. Phys.* **14**, 12404–12422 (2012).
260. Dixon, J. M., Taniguchi, M. & Lindsey, J. S. PhotoChemCAD 2: a refined program with accompanying spectral databases for photochemical calculations. *Photochem. Photobiol.* **81**, 212–213 (2005).
261. Caselli, P., Myers, P. C. & Thaddeus, P. Radio-astronomical spectroscopy of the hyperfine structure of  $\text{N}_2\text{H}^+$ . *Astrophys. J.* **455**, L77–L80 (1995).
262. Neese, F. Sum-over-states based multireference ab initio calculation of EPR spin Hamiltonian parameters for transition metal complexes. A case study. *Magn. Reson. Chem.* **42**, S187–S198 (2004).

### Acknowledgements

In Italy, the work described in this Primer was supported by MIUR PRIN funds (grants 2015F59J3R, 2017A4XRCA), the Italian Space Agency (ASI) ('Life in Space' project, N. 2019-3-U.0) and SMART@SNS Laboratory for high-performance computing facilities. F.N. is extremely grateful for generous financial support by the Max Planck Society that enables us to follow curiosity-driven research. The science described in this Primer has also been supported by the German Science Foundation through the cluster of excellence programme Gefördert durch die Deutsche Forschungsgemeinschaft (DFG) im Rahmen der Exzellenzstrategie des Bundes und der Länder – EXC 2035 – Projektnummer 390677874. A.B.M. and R.J.D. thank National Science Foundation (NSF) CHE-1856125; R.J.D. was supported by a fellowship from The Molecular Sciences Software Institute under NSF grant OAC-1547580.

### Author contributions

Introduction (V.B., M.B., F.N. and C.P.); Experimentation (V.B., M.B., J.R.C., A.B.M., F.N. and C.P.); Results (M.M., C.P., V.B., M.B., A.B.M., R.J.D. and J.R.C.); Applications (M.M., C.P., D.C.C. and F.N.); Reproducibility and data deposition (S.A., V.B., M.B., A.B.M. and C.P.); Limitations and optimizations (S.A., V.B., M.B., J.R.C. and C.P.); Outlook (V.B.); Overview of the Primer (C.P.).

### Competing interests

The authors declare no competing interests.

### Peer review information

*Nature Reviews Methods Primers* thanks M. Hanson-Heine, J. Kästner, J. Tennyson and the other anonymous reviewer(s) for their contribution to the peer review of this work.

### Publisher's note

Springer Nature remains neutral with regard to jurisdictional claims in published maps and institutional affiliations.

### Supplementary information

The online version contains supplementary material available at <https://doi.org/10.1038/s43586-021-00034-1>.

### RELATED LINKS

- CFOUR: <http://www.cfour.de/>
- Database of semi-experimental equilibrium structures: <https://smart.sns.it/molecules/>
- Gaussian: <https://gaussian.com/>
- Molpro: <https://www.molpro.net>
- MolSSI workshop: <https://molssi.org/2019/08/19/molssi-workshop-rovibrational-molecular-spectroscopy/>
- NWCHEM: <https://nwchemgit.github.io/>
- ORCA (academic): <https://orcaforum.kofo.mpg.de/app.php/portal>
- ORCA (commercial): <https://www.faccs.de>
- PSI4: <http://www.psi4code.org>
- QChem: <http://www.q-chem.com/>
- SMART@SNS Laboratory: <http://smart.sns.it>